Relativistic many-body calculations of the energies of $n=4$ states along the zinc isoelectronic sequence

S. A. Blundell*
Département de Recherche Fondamentale sur la Matière Condensée, CEA-Grenoble/DSM, 17 rue des Martyrs, F-38054 Grenoble Cedex 9, France

W. R. Johnson†
Department of Physics, University of Notre Dame, Notre Dame, Indiana 46556, USA

M. S. Safronova‡
Department of Physics and Astronomy, 217 Sharp Lab, University of Delaware, Newark, Delaware 19716, USA

U. I. Safronova§
Physics Department, University of Nevada, Reno, Nevada 89557, USA
(Received 12 January 2008; published 14 March 2008)

The energies of the 44 even-parity and 40 odd-parity ($4l4l'$) states of ions of the zinc isoelectronic sequence are determined through second order in relativistic many-body perturbation theory. Our calculations start from a Ni-like $V^{(N-2)}$ Dirac-Fock potential. Two alternative treatments of the Breit interaction are investigated. In the first approach, we omit Breit contributions to the Dirac-Fock potential and evaluate Coulomb and Breit-Coulomb corrections through second order perturbatively. This approach was used previously to evaluate the energies of Be-, B-, Mg-, and Yb-like systems. In the second approach, we include both Coulomb and Breit contributions to the Breit-Dirac-Fock potential and then treat the residual Breit and Coulomb interactions perturbatively. The results obtained from the two approaches are compared and discussed. Theoretical excitation energies are compared with critically evaluated experimental data and with results from other recent calculations. Trends of excitation energies including splitting of triplet terms as functions of nuclear charge $Z=34-100$ are illustrated graphically for some states. The resulting Z dependence shows explicitly the effect of mixing of $[4p^2+4s4d]$, $[4d^2+4p4f]$, and $[4p4d+4s4f]$ configurations.

DOI: 10.1103/PhysRevA.77.032507 PACS number(s): 31.15.A−, 31.15.am, 31.15.vj, 31.30.J−

I. INTRODUCTION

Multiconfiguration Dirac-Fock (MCDF) calculations for the lowest excited states in the Zn-like sequence were recently presented by Liu *et al.* in Ref. [1]. A project to apply relativistic many-body perturbation theory (RMBPT) to two-valence-electron systems was started about ten years ago, and Be-, Mg-, Ca-, and Yb-like ions have been investigated by this method in Refs. [2–5]. Generally, RMBPT calculations based on a Dirac-Fock basis set and first-order RMBPT give results of comparable accuracy to those obtained from MCDF codes, while the second-order RMBPT used in the above-mentioned papers gives results beyond the MCDF approach. In the present paper, we use the RMBPT technique to evaluate the energies of the $4l4l'$ states of Zn-like ions.

The $4s^2\ {}^1S_0-4s4p\ {}^1P_1$ transitions of ten Zn-like ions from Ba^{26+} to W^{44+}, observed by means of a laser-produced plasma and a 2.2-m grazing-incidence spectrograph, were presented by Reader and Luther [6]. Some years later the $4s^2\ {}^1S_0-4s4p\ {}^1P_1$ transitions of 29 Zn-like ions from Ru^{14+} to Dy^{36+}, observed in a laser-produced plasma and a 10.7-m grazing-incidence spectrograph, were reported by Acquista and Reader [7]. Spectra of very highly charged ions of Au^{49+}, Pb^{52+}, Bi^{53+}, Th^{60+}, and U^{62+} were observed in laser-produced plasmas generated by the OMEGA laser by Seely *et al.* [8]. The agreement between the measured transition energies and the transition energies calculated within the MCDF approximation (Grant code) was observed to improve with increasing Z [8]. The intercombination lines of the zinc sequence corresponding to the transition $4s^2\ {}^1S_0-4s4p\ {}^3P_1$, observed for Xe^{24+}, La^{27+}, Nd^{30+}, Eu^{33+}, Gd^{34+}, and Yb^{40+} in the Princeton Large Torus tokamak discharge, were presented by Hinnov *et al.* [9]. Spectra of the Zn-like ions Rb VIII–Mo XIII were excited with sparks and laser-produced plasmas by Litzen and Reader in Ref. [10]. The observed energy levels of the $4s^2$, $4s4p$, $4p^2$, $4s4d$, $4s5s$, $4s5p$, $4s5d$, and $4p5s$ configurations were interpreted by means of least-squares parameter fits and Hartree-Fock calculations. An identification of $n=4$, $\Delta n=0$ transitions in the spectra of zinc-like ions from $Z=37$ (Rb^{9+}) to $Z=50$ (Sn^{22+}) was reported by Churilov *et al.* in Ref. [11]. The spectra were excited in a laser-produced plasma. The transition arrays $(4s^2+4p^2+4s4d)-4s4p$ were identified with the help of the *ab initio* relativistic parametric potential method and the Slater-Condon method with generalized least-squares fits of energy parameters. Analysis of the spectrum of the Zn-like Kr^{6+} ion for highly excited $4p4d$ and $4p5s$ configurations was reported by Churilov in Ref. [12]. The spectrum of the Zn-like

*steven.blundell@cea.fr
†johnson@nd.edu
‡msafrono@udel.edu
§On leave from ISAN, Troitsk, Russia. usafrono@nd.edu

TABLE I. Possible two-particle states in the $4lj4l'j'$ complexes; *jj*- and *LS*-coupling schemes.

$J=0,1$		$J=2$		$J=3$		$J=4,5,6$	
jj coupl.	*LS* coupl.	*jj* coupl.	*LS* coupl.	*jj* coupl.	*LS* coupl.	*jj* coupl.	*LS* coupl.
			Odd-parity states				
$4s_{1/2}4p_{1/2}(0)$	$4s4p\ ^3P_0$	$4s_{1/2}4p_{3/2}(2)$	$4s4p\ ^3P_2$	$4p_{1/2}4d_{5/2}(3)$	$4p4d\ ^3D_3$	$4p_{3/2}4d_{5/2}(4)$	$4p4d\ ^3F_4$
$4p_{3/2}4d_{3/2}(0)$	$4p4d\ ^3P_0$	$4p_{1/2}4d_{3/2}(2)$	$4p4d\ ^1D_2$	$4p_{3/2}4d_{3/2}(3)$	$4p4d\ ^3F_3$	$4s_{1/2}4f_{7/2}(4)$	$4s4f\ ^3F_4$
$4d_{5/2}4f_{5/2}(0)$	$4d4f\ ^3P_0$	$4p_{1/2}4d_{5/2}(2)$	$4p4d\ ^3D_2$	$4p_{3/2}4d_{5/2}(3)$	$4p4d\ ^1F_3$	$4d_{3/2}4f_{5/2}(4)$	$4d4f\ ^iG_4$
$4s_{1/2}4p_{1/2}(1)$	$4s4p\ ^3P_1$	$4p_{3/2}4d_{3/2}(2)$	$4p4d\ ^3F_2$	$4s_{1/2}4f_{5/2}(3)$	$4s4p\ ^3F_3$	$4d_{3/2}4f_{7/2}(4)$	$4d4f\ ^3H_4$
$4s_{1/2}4p_{3/2}(1)$	$4s4p\ ^1P_1$	$4p_{3/2}4d_{5/2}(2)$	$4p4d\ ^3P_2$	$4s_{1/2}4f_{7/2}(3)$	$4s4p\ ^1F_3$	$4d_{5/2}4f_{5/2}(4)$	$4d4f\ ^3F_4$
$4p_{1/2}4d_{3/2}(1)$	$4p4d\ ^3D_1$	$4s_{1/2}4f_{5/2}(2)$	$4s4p\ ^3F_2$	$4d_{3/2}4f_{5/2}(3)$	$4d4f\ ^3F_3$	$4d_{5/2}4f_{7/2}(4)$	$4d4f\ ^3G_4$
$4p_{3/2}4d_{3/2}(1)$	$4p4d\ ^3P_1$	$4d_{3/2}4f_{5/2}(2)$	$4d4f\ ^3F_2$	$4d_{3/2}4f_{7/2}(3)$	$4d4f\ ^3G_3$	$4d_{3/2}4f_{7/2}(5)$	$4d4f\ ^3H_5$
$4p_{3/2}4d_{5/2}(1)$	$4p4d\ ^1P_1$	$4d_{3/2}4f_{7/2}(2)$	$4d4f\ ^1D_2$	$4d_{5/2}4f_{5/2}(3)$	$4d4f\ ^3D_3$	$4d_{5/2}4f_{5/2}(5)$	$4d4f\ ^3G_5$
$4d_{3/2}4f_{5/2}(1)$	$4d4f\ ^3D_1$	$4d_{5/2}4f_{5/2}(2)$	$4d4f\ ^3D_2$	$4d_{5/2}4f_{7/2}(3)$	$4d4f\ ^1F_3$	$4d_{5/2}4f_{7/2}(5)$	$4d4f\ ^1H_5$
$4d_{5/2}4f_{5/2}(1)$	$4d4f\ ^3P_1$	$4d_{5/2}4f_{7/2}(2)$	$4d4f\ ^3P_2$			$4d_{5/2}4f_{7/2}(6)$	$4d4f\ ^3H_6$
$4d_{5/2}4f_{7/2}(1)$	$4d4f\ ^1P_1$						
			Even-parity states				
$4s_{1/2}4s_{1/2}(0)$	$4s^2\ ^1S_0$	$4p_{1/2}4p_{3/2}(2)$	$4p^2\ ^3P_2$	$4s_{1/2}4d_{5/2}(3)$	$4s4d\ ^3D_3$	$4p_{1/2}4f_{7/2}(4)$	$4p4f\ ^3F_4$
$4p_{1/2}4p_{1/2}(0)$	$4p^2\ ^3P_0$	$4p_{3/2}4p_{3/2}(2)$	$4p^2\ ^1D_2$	$4p_{1/2}4f_{5/2}(3)$	$4p4f\ ^3F_3$	$4p_{3/2}4f_{5/2}(4)$	$4p4f\ ^1G_4$
$4p_{3/2}4p_{3/2}(0)$	$4p^2\ ^1S_0$	$4s_{1/2}4d_{3/2}(2)$	$4s4d\ ^3D_2$	$4p_{1/2}4f_{7/2}(3)$	$4p4f\ ^1F_3$	$4p_{3/2}4f_{7/2}(4)$	$4p4f\ ^3G_4$
$4d_{3/2}4d_{3/2}(0)$	$4d^2\ ^3P_0$	$4s_{1/2}4d_{5/2}(2)$	$4s4d\ ^1D_2$	$4p_{3/2}4f_{5/2}(3)$	$4p4f\ ^3G_3$	$4d_{3/2}4d_{5/2}(4)$	$4d^2\ ^3F_4$
$4d_{5/2}4d_{5/2}(0)$	$4d^2\ ^1S_0$	$4p_{1/2}4f_{5/2}(2)$	$4p4f\ ^3F_2$	$4p_{3/2}4f_{7/2}(3)$	$4p4f\ ^3D_3$	$4d_{5/2}4d_{5/2}(4)$	$4d^2\ ^1G_4$
$4f_{5/2}4f_{5/2}(0)$	$4f^2\ ^3P_0$	$4p_{3/2}4f_{5/2}(2)$	$4p4f\ ^1D_2$	$4d_{3/2}4d_{5/2}(3)$	$4d^2\ ^3F_3$	$4f_{5/2}4f_{5/2}(4)$	$4f^2\ ^3H_4$
$4f_{7/2}4f_{7/2}(0)$	$4f^2\ ^1S_0$	$4p_{3/2}4f_{7/2}(2)$	$4p4f\ ^3D_2$	$4f_{5/2}4f_{7/2}(3)$	$4f^2\ ^3F_3$	$4f_{5/2}4f_{7/2}(4)$	$4f^2\ ^3F_4$
$4p_{1/2}4p_{3/2}(1)$	$4p^2\ ^3P_1$	$4d_{3/2}4d_{3/2}(2)$	$4d^2\ ^3F_2$			$4f_{7/2}4f_{7/2}(4)$	$4f^2\ ^1G_4$
$4s_{1/2}4d_{3/2}(1)$	$4s4d\ ^3D_1$	$4d_{5/2}4d_{5/2}(2)$	$4d^2\ ^3P_2$			$4p_{3/2}4f_{7/2}(5)$	$4p4f\ ^3G_5$
$4p_{3/2}4f_{5/2}(1)$	$4p4f\ ^3D_1$	$4d_{3/2}4d_{5/2}(2)$	$4d^2\ ^1D_2$			$4f_{3/2}4f_{7/2}(5)$	$4f^2\ ^3H_5$
$4d_{3/2}4d_{5/2}(1)$	$4d^2\ ^3P_1$	$4f_{5/2}4f_{5/2}(2)$	$4f^2\ ^3F_2$			$4f_{3/2}4f_{7/2}(6)$	$4f^2\ ^3H_6$
$4f_{5/2}4f_{7/2}(1)$	$4f^2\ ^3P_1$	$4f_{5/2}4f_{7/2}(2)$	$4f^2\ ^1D_2$			$4f_{7/2}4f_{7/2}(6)$	$4f^2\ ^1I_6$
		$4f_{7/2}4f_{7/2}(2)$	$4f^2\ ^3P_2$				

Kr^{6+} ion, excited in a capillary discharge and recorded with a high-resolution spectrometer, was also studied. The $(4p^2+4s4d)$-$4p4d$ and $(4p^2+4s5s)$-$4p5s$ transitions were identified in Ref. [12] for the first time. The results of the analysis performed were confirmed by semiempirical calculations in terms of the Hartree-Fock method.

New measurements of the Zn-like resonance lines $4s^2\ ^1S_0-4s4p\ ^{1,3}P_1$ of Pd^{16+} to Dy^{36+}, with an uncertainty of ± 0.005 Å, were reported by Sugar *et al.* in Ref. [13]. The light source was the TEXT tokamak at the Fusion Research Center in Austin, Texas. The transition energies for the Zn-like ions were compared with values calculated with the multiconfiguration Dirac-Fock code of Indelicato and Desclaux [14]. The difference in wavelengths between experimental and theoretical values decreases with Z: a deviation of 1.1% was found for Pd^{16+} and 0.4% for Dy^{36+}. Measurements of the resonance lines $4s^2\ ^1S_0-4s4p\ ^{1,3}P_1$ of Er^{38+} and Hf^{42+} were reported by Sugar *et al.* in Ref. [15]. Spectra of these ions were observed by injecting the corresponding elements into the plasma of the TEXT tokamak.

Using an electron-beam ion trap and a flat-field spectrometer, the $4s^2\ ^1S_0-4s4p\ ^1P_1$ resonance lines of Zn-like ions of Yb^{40+}, W^{44+}, Au^{49+}, Pb^{52+}, Th^{60+}, and U^{62+} were observed and their wavelengths measured with greatly improved accuracy by Utter *et al.* in Ref. [16]. The experimental results were compared to those from laser-produced plasmas and to theory, and significant differences were found [16]. The $4s^2\ ^1S_0-4s4p\ ^1P_1$ resonance lines of Zn-like ions of Os^{46+}, Bi^{83+}, Th^{60+}, and U^{62+} were also observed in an electron-beam ion trap and their wavelengths measured using a high-resolution flat-field spectrometer by Träbert *et al.* [17]. The spectral resolution in Ref. [17] was 3–6 times better than earlier measurements; however, substantial disagreement was found with theoretical predictions.

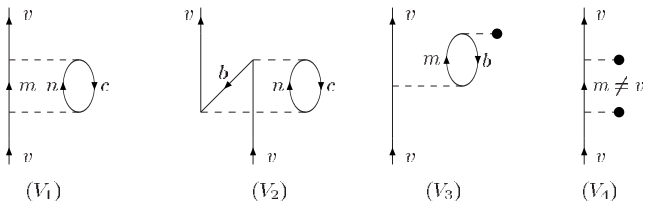

FIG. 1. Diagrams for the contributions of $E_v^{(2)}$ to the second-order two-particle energy. V_1 represents double sums over virtual intermediate states, V_2 represents single sums, V_3 gives one-potential terms, and V_4 gives two-potential terms.

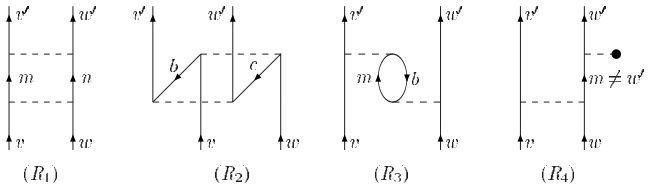

FIG. 2. Diagrams for the second-order interaction energy $V^{(2)}_{v'w'vw}$. R_1 represents double sums over virtual intermediate states, R_2 represents single sums, R_3 gives RPA terms, and R_4 gives one-potential terms.

A detailed theoretical investigation of the energy levels for the $n=4$, $\Delta n=0$ transitions of the ions Rb^{7+} to Xe^{24+} along the zinc isoelectronic sequence using the relativistic Hartree-Fock method (Cowan code) was presented by Biémont *et al.* in Ref. [18]. All configurations within the $n=4$ complex, both even and odd parities, were included in the calculations. Using a well-established least-squares fitting procedure, the average energies, Slater integrals, and spin-orbit parameters were adjusted to obtain the best agreement between calculated and established energy levels for ions with $Z \leq 90$.

Cheng and Wagner [19] compared multiconfiguration Dirac-Fock energies with experiment for the $4s^2\ ^1S_0 - 4s4p\ ^1P_1$ transition of the Zn-like ions Au^{49+}, Pb^{52+}, Bi^{53+}, Th^{60+}, and U^{62+}. The Coulomb, Breit, and quantum electrodynamic (QED) corrections to $4p$-$4d$ transitions were tabulated for selected ions in the range $Z=50-92$. The agreement found between theory and experiment was good enough to show the importance of QED corrections in the spectra of these highly stripped ions [19].

The atomic structure of the low-energy configurations of the Zn-like ions Rb^{7+} to W^{44+} was analyzed in detail by Biémont in Ref. [20]. A MCDF technique was used to investigate the level crossings and compositions in the $n=4$ configurations. Level energies, wavelengths, transitions probabilities, and oscillator strengths were tabulated for Ag^{17+} to W^{44+} [20].

Calculated and experimentally determined transition energies were presented for the Zn isoelectronic sequence for the elements with atomic numbers $Z=50-92$ by Brown *et al.* in Ref. [21]. The excitation energies were calculated for the 84 levels belonging to the 10 configurations of the type $4l4l'$ by using the Hebrew University Lawrence Livermore Atomic Code (HULLAC). The differences between the calculated and experimental transition energies were determined for 16 transitions, and the excitation energies of the levels belonging to the $4s4p$, $4p^2$, $4s4d$, and $4s4f$ configurations were derived from the semiempirically corrected transition energies [21].

Chou *et al.* [22] presented the $4s^2\ ^1S_0 - 4s4p\ ^{1,3}P_1$ excitation energies in Zn-like ions, calculated by using the multiconfiguration relativistic random-phase approximation including excitation channels from core electrons. The disagreement between theory and experiment was reduced, but discrepancies remained.

High-accuracy calculations of term energies and wavelengths of resonance lines in Zn-like ions were performed by Vilkas and Ishikawa in Ref. [23] using relativistic multireference Møller-Plesset (MR-MP) perturbation theory.

In this paper, RMBPT through second order is used to calculate energies of the $4s^2$, $4p^2$, $4d^2$, $4f^2$, $4s4d$, and $4p4f$ even-parity states and the $4s4p$, $4s4f$, $4p4d$, and $4d4f$ odd-parity states of ions of the zinc isoelectronic sequence for a wide range of nuclear charges, $Z=30-100$. Two alternative treatments of the Breit interaction are investigated. In the first approach, we omit Breit contributions to the Dirac-Fock potential and evaluate Coulomb and Breit-Coulomb corrections through second order perturbatively. This approach was used previously to evaluate energies of Be-, B-, Mg-, and Yb-like systems. In the second approach, we include both Coulomb and Breit contributions in the Breit-Dirac-Fock potential and then treat the residual Breit and Coulomb interactions perturbatively. QED corrections are inferred by a combination of phenomenological and *ab initio* methods.

II. THEORETICAL TECHNIQUE

The RMBPT formalism developed previously [2–5] for Be-, Mg-, Ca-, and Yb-like ions is used here to obtain second-order energies. Differences in the calculation procedure for Be-, Mg-, and Zn-like ions arise from the increased size of the model space ($4l4l'$ instead of $3l3l'$ and $2l2l'$ for Mg- and Be-like ions, respectively) and the Dirac-Fock potential ($1s^22s^22p^63s^23p^63d^{10}$ instead of $1s^22s^22p^6$ and $1s^2$

TABLE II. Contributions to the valence-electron energy $E^{(2)}_v$ (a.u.) for $v=4s$, $4p_j$, $4d_j$, and $4f_j$ for ions with a Ni-like core from the three diagrams V_1-V_3 evaluated for the case of xenon, $Z=54$. Notation: $a[b]$ represents $a\times 10^b$.

	Coulomb Interaction:		Breit-Coulomb Correction		
$4lj$	V_1	V_2	BV_1	BV_2	BV_3
$4s_{1/2}$	−7.875[−2]	1.670[−2]	−5.017[−4]	1.484[−4]	−6.667[−3]
$4p_{1/2}$	−8.025[−2]	1.744[−2]	−6.873[−4]	1.786[−4]	−6.919[−3]
$4p_{3/2}$	−7.529[−2]	1.726[−2]	−6.231[−4]	1.486[−4]	−6.728[−3]
$4d_{3/2}$	−7.769[−2]	1.707[−2]	−6.800[−4]	2.847[−4]	−7.191[−3]
$4d_{5/2}$	−7.609[−2]	1.700[−2]	−6.480[−4]	2.234[−4]	−7.157[−3]
$4f_{5/2}$	−6.486[−2]	1.119[−2]	−4.872[−4]	3.063[−4]	−4.172[−3]
$4f_{7/2}$	−6.400[−2]	1.137[−2]	−3.790[−4]	2.111[−4]	−4.008[−3]

TABLE III. Diagonal and off-diagonal contributions to the second-order interaction term (a.u.) in the effective Hamiltonian matrix from diagrams R_1-R_3 calculated using DF orbitals. These contributions are given for a two-electron ion with a Ni-like core and evaluated numerically for the case of xenon, $Z=54$. Notation: $a[b]$ represents $a\times10^b$.

			Coulomb Interaction			Breit-Coulomb Correction			
$4l_1j_14l_2j_2$	$4l_3j_34l_4j_4$	J	R_1	R_2	R_3	BR_1	BR_2	BR_3	BR_4
$4s_{1/2}4s_{1/2}$	$4s_{1/2}4s_{1/2}$	0	−1.232[−2]	−4.912[−4]	−1.122[−2]	−4.105[−5]	−1.014[−5]	−5.473[−7]	−9.909[−4]
$4p_{1/2}4p_{1/2}$	$4p_{1/2}4p_{1/2}$	0	−1.388[−2]	−5.217[−4]	−1.157[−2]	−6.230[−5]	−1.056[−5]	1.231[−5]	−1.626[−3]
$4p_{3/2}4p_{3/2}$	$4p_{3/2}4p_{3/2}$	0	−1.919[−2]	−7.845[−4]	−1.268[−2]	−1.067[−4]	−2.046[−5]	1.153[−5]	−1.241[−3]
$4d_{3/2}4d_{3/2}$	$4d_{3/2}4d_{3/2}$	0	−2.610[−2]	−8.734[−4]	−1.387[−2]	−1.814[−4]	−2.117[−5]	3.975[−5]	−1.105[−3]
$4d_{5/2}4d_{5/2}$	$4d_{5/2}4d_{5/2}$	0	−3.167[−2]	−1.076[−3]	−1.346[−2]	−2.407[−4]	−2.999[−5]	4.016[−5]	−8.081[−4]
$4f_{5/2}4f_{5/2}$	$4f_{5/2}4f_{5/2}$	0	−5.191[−2]	−1.531[−3]	−5.151[−3]	−3.886[−4]	−3.393[−5]	7.237[−5]	−7.014[−4]
$4f_{7/2}4f_{7/2}$	$4f_{7/2}4f_{7/2}$	0	−5.759[−2]	−1.897[−3]	−3.327[−3]	−4.620[−4]	−2.890[−5]	5.639[−5]	−4.280[−4]
$4s_{1/2}4s_{1/2}$	$4p_{1/2}4p_{1/2}$	0	8.070[−3]	3.825[−4]	2.394[−2]	4.743[−5]	1.013[−5]	1.688[−5]	1.818[−4]
$4p_{1/2}4p_{1/2}$	$4s_{1/2}4s_{1/2}$	0	6.786[−3]	3.606[−4]	2.186[−2]	4.207[−5]	9.652[−6]	1.566[−5]	2.591[−4]
$4s_{1/2}4s_{1/2}$	$4p_{3/2}4p_{3/2}$	0	1.145[−2]	5.399[−4]	3.373[−2]	7.490[−5]	1.563[−5]	1.011[−5]	2.289[−4]
$4p_{3/2}4p_{3/2}$	$4s_{1/2}4s_{1/2}$	0	9.109[−3]	4.986[−4]	2.982[−2]	6.261[−5]	1.463[−5]	8.612[−6]	3.553[−4]
$4s_{1/2}4s_{1/2}$	$4d_{3/2}4d_{3/2}$	0	−1.284[−2]	−4.230[−4]	−3.957[−3]	−1.104[−4]	−1.207[−5]	3.927[−6]	−6.768[−5]
$4d_{3/2}4d_{3/2}$	$4s_{1/2}4s_{1/2}$	0	−6.581[−3]	−3.529[−4]	−3.122[−3]	−5.332[−5]	−1.037[−5]	3.080[−6]	−3.361[−4]
$4s_{1/2}4s_{1/2}$	$4d_{5/2}4d_{5/2}$	0	−1.635[−2]	−5.227[−4]	−4.709[−3]	−1.367[−4]	−1.575[−5]	1.127[−5]	−7.619[−5]
$4d_{5/2}4d_{5/2}$	$4s_{1/2}4s_{1/2}$	0	−8.106[−3]	−4.335[−4]	−3.691[−3]	−6.701[−5]	−1.328[−5]	9.540[−6]	−4.165[−4]
$4s_{1/2}4s_{1/2}$	$4f_{5/2}4f_{5/2}$	0	8.353[−3]	6.994[−4]	−3.339[−3]	7.689[−5]	1.407[−5]	−1.799[−5]	5.939[−5]
$4f_{5/2}4f_{5/2}$	$4s_{1/2}4s_{1/2}$	0	6.740[−3]	5.309[−4]	−1.732[−3]	5.680[−5]	1.055[−5]	−1.104[−5]	3.985[−5]
$4s_{1/2}4s_{1/2}$	$4f_{7/2}4f_{7/2}$	0	9.373[−3]	8.279[−4]	−4.247[−3]	9.810[−5]	1.393[−5]	−3.321[−5]	7.633[−5]
$4f_{7/2}4f_{7/2}$	$4s_{1/2}4s_{1/2}$	0	7.880[−3]	6.258[−4]	−2.186[−3]	6.906[−5]	1.035[−5]	−1.898[−5]	6.242[−5]
$4s_{1/2}4p_{1/2}$	$4s_{1/2}4p_{1/2}$	1	−1.116[−2]	−3.244[−4]	−3.691[−3]	−1.720[−5]	−1.424[−6]	−9.082[−6]	−1.234[−3]
$4s_{1/2}4p_{3/2}$	$4s_{1/2}4p_{3/2}$	1	−1.635[−2]	−5.108[−4]	−1.808[−2]	−5.090[−5]	−6.072[−6]	−1.817[−5]	−1.139[−3]
$4p_{1/2}4d_{3/2}$	$4p_{1/2}4d_{3/2}$	1	−2.080[−2]	−4.624[−4]	−1.868[−2]	−8.134[−5]	−4.642[−6]	−2.348[−6]	−1.378[−3]
$4p_{3/2}4d_{3/2}$	$4p_{3/2}4d_{3/2}$	1	−1.370[−2]	−3.126[−4]	−1.389[−2]	−2.939[−5]	−2.219[−6]	−9.253[−6]	−1.062[−3]
$4p_{3/2}4d_{5/2}$	$4p_{3/2}4d_{5/2}$	1	−2.759[−2]	−6.182[−4]	−1.539[−2]	−1.268[−4]	−8.716[−6]	−1.102[−5]	−1.033[−3]
$4d_{3/2}4f_{5/2}$	$4d_{3/2}4f_{5/2}$	1	−3.750[−2]	−4.377[−5]	−1.261[−2]	−1.343[−4]	−2.922[−6]	7.727[−6]	−9.562[−4]
$4d_{5/2}4f_{5/2}$	$4d_{5/2}4f_{5/2}$	1	−2.936[−2]	−3.442[−5]	−1.259[−2]	−8.850[−5]	−2.529[−6]	−4.037[−6]	−7.089[−4]
$4d_{5/2}4f_{7/2}$	$4d_{5/2}4f_{7/2}$	1	−5.000[−2]	−6.501[−5]	−1.122[−2]	−2.541[−4]	−2.665[−6]	−5.673[−6]	−6.759[−4]
$4s_{1/2}4p_{1/2}$	$4s_{1/2}4p_{3/2}$	1	−7.735[−3]	−2.764[−4]	−2.165[−2]	−2.964[−5]	−3.648[−6]	−1.997[−5]	−1.958[−4]
$4s_{1/2}4p_{3/2}$	$4s_{1/2}4p_{1/2}$	1	−7.508[−3]	−2.738[−4]	−2.131[−2]	−2.915[−5]	−3.617[−6]	−1.979[−5]	−2.081[−4]
$4s_{1/2}4p_{1/2}$	$4p_{1/2}4d_{3/2}$	1	−9.549[−3]	−2.403[−4]	−2.203[−2]	−4.455[−5]	−4.065[−6]	−2.015[−5]	−1.652[−4]
$4p_{1/2}4d_{3/2}$	$4s_{1/2}4p_{1/2}$	1	−7.207[−3]	−2.205[−4]	−1.921[−2]	−3.589[−5]	−3.793[−6]	−1.800[−5]	−2.833[−4]

for Mg- and Be-like ions, respectively). These differences lead to much more laborious numerical calculations (84 states compared to 35 states in Mg-like ions and 10 in Be-like ions).

For atoms with two electrons outside closed shells, the model space is formed from two-particle states of the type $a_v^\dagger a_w^\dagger|0\rangle$, where $|0\rangle$ is the ground-state determinant of the closed-shell core with $N-2$ electrons. The single-particle indices v and w range over states in the valence shell. For our study of low-lying states of Zn-like ions, v and w are the $4s_{1/2}$, $4p_{1/2}$, $4p_{3/2}$, $4d_{3/2}$, $4d_{5/2}$, $4f_{5/2}$, and $4f_{7/2}$ single-particle states.

The model space for the $n=4$ complex in Zn-like ions has 44 even-parity states and 40 odd-parity states. These states are summarized in Table I, where both jj and LS designations are given. When starting calculations from relativistic Dirac-Fock wave functions, it is natural to use jj designations for uncoupled transition and energy matrix elements; however, neither jj nor LS coupling describes the *physical* states properly, except for the single-configuration state $4d_{5/2}4f_{7/2}(6)\equiv 4d4f\ ^3H_6$.

The second-order effective Hamiltonian can be written

$$\langle\Phi_{JM}(v'w')|H^{(2)}|\Phi_{JM}(vw)\rangle=\delta_{vv'}\delta_{ww'}(E_v^{(2)}+E_w^{(2)})+V_{v'w'vw}^{(2)}. \quad (1)$$

Analytical expressions for the second-order one-particle valence contribution $E_v^{(2)}$ and two-particle correlation contribution $V_{v'w'vw}^{(2)}$ were presented by Safronova *et al.* [2]. The second-order $E_v^{(2)}$ term consists of four contributions, V_1, V_2, V_3, and V_4, represented in terms of Bruckner-Goldstone dia-

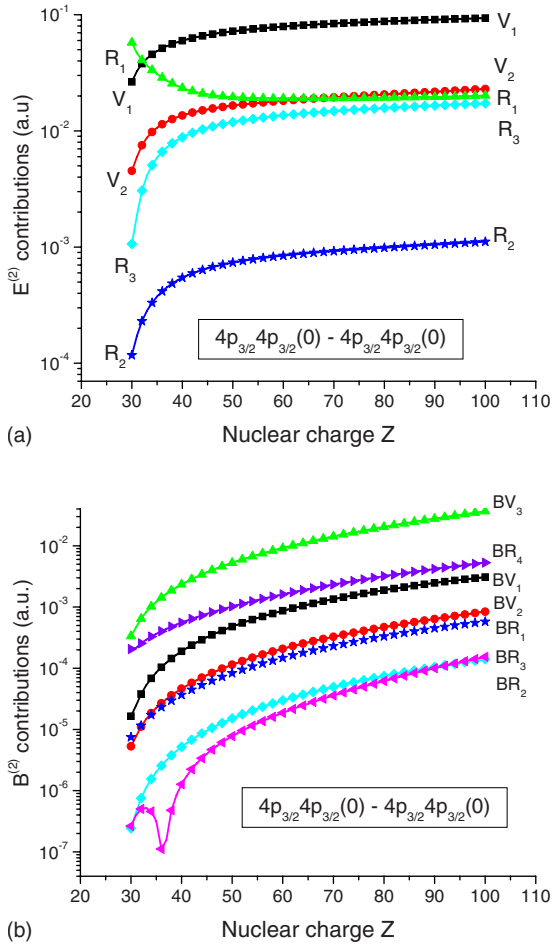

FIG. 3. (Color online) Contributions to the second-order $(4p_{3/2}^2)-(4p_{3/2}^2)[J=0]$ diagonal matrix element for the DF potential: (a) Coulomb interaction $E_{\mathrm{DF}}^{(2)}$, (b) Breit interaction $B_{\mathrm{DF}}^{(2)}$.

grams in Fig. 1. V_1 represents double sums over virtual intermediate states, V_2 represents single sums, V_3 gives one-potential terms, and V_4 gives two-potential terms. The dashed lines designate Coulomb plus Breit interactions. Diagrams for the second-order two-particle energy $V_{v'w'vw}^{(2)}$ are given in Fig. 2. R_1 represents double sums, R_2 represents single sums, R_3 gives random-phase-approximation (RPA) terms, and R_4 gives one-potential terms.

A. Example: Energy matrix for Xe^{14+}

In Tables II and III, we give details of the second-order contributions to the energies for the special case of Zn-like xenon, $Z=54$. In Table II, we show the second-order contributions to the valence energy $E_v^{(2)}$. Contributions from the various diagrams in Fig. 1 are given in this table for the case of a DF potential (excluding Breit terms) and a perturbative treatment of the Breit interaction through first order. In this case, the one-potential operator, represented by a solid circle in Fig. 1, contains contributions only from the Breit interaction [2]. Thus, to first order in the Breit interaction, diagram V_4 does not contribute. However, one should note that when using non-DF orbitals, the Coulomb interaction also contributes to the one-potential operator. Indeed, for hydrogenic orbitals V_4 can give the largest contribution among the four valence diagrams (for details, see Ref. [2]). As to the V_3 diagram, it follows that this gives a Breit-Coulomb contribution of first order in the Breit interaction, but no Coulomb-Coulomb contribution. Noting that the dashed line corresponds to the sum of the Coulomb and Breit interactions, one sees that diagrams V_1 and V_2 can give both Coulomb-Coulomb and Breit-Coulomb contributions. To summarize, the second-order Coulomb-Coulomb contributions are represented by two diagrams V_1 and V_2 and the Breit-Coulomb contributions by three diagrams BV_1, BV_2, and BV_3 (see Table II). We can see from this table that the largest contribution to the second-order valence energy $E_v^{(2)}$ is the double-sum diagram V_1. The single-sum diagram V_2 compensates the V_1 contribution by a factor of 1/5. A substantial contribution to $E_v^{(2)}$ from Breit-Coulomb operators arises only from BV_3. The other two terms BV_1 and BV_2 are smaller than the dominant V_1 term by two orders of magnitude.

Table III gives the second-order interaction energy, shown in Fig. 2, for the special case $Z=54$. These diagrams contribute for systems with two (or more) electrons above a closed core. There are 84 diagonal and 580 nondiagonal matrix elements for $(4l4l')[J]$ states in jj coupling. We calculated contributions for the 664 matrix elements using DF orbitals. We illustrate our results by 17 even-parity matrix elements with $J=0$ and 14 odd-parity matrix elements with $J=1$ in Table III. This table includes data of three diagrams from Coulomb-Coulomb operators and four diagrams from Breit-Coulomb operators for the second-order two-particle energy, $V_{v'w'vw}^{(2)}$. As can be seen from Table III, the largest contributions to the value of $V_{v'w'vw}^{(2)}$ are from the double sums (diagram R_1 and R_3 representing the RPA contribution). The largest contribution among diagrams BR_1-BR_4 describing the second-order Breit-Coulomb terms are the one-potential terms represented by the BR_4 diagram. It should be noted that the R_4 contributions vanish in the case of the Coulomb-Coulomb operator [2]. As one can see from Table III, the ratio of off-diagonal and diagonal matrix elements is 0.1–0.5 for most cases. Note that the off-diagonal matrix elements are not symmetric; the values of the $R_{(i)}[v'w'(J),vw(J)]$ and $R_{(i)}[vw(J),v'w'(J)]$ matrix elements differ in some cases by a factor of 2–3 and occasionally have opposite signs.

The orbitals used in the present calculations were obtained as linear combinations of B-splines. These B-spline basis orbitals were determined using precisely the method described in Ref. [26]. We used 50 B-splines of order 9 for each single-particle angular momentum state, and we included all orbitals with orbital angular momentum $l\leq 9$ in our single-particle basis.

B. Z dependence of diagram contributions

In Fig. 3 we illustrate the Z dependence of the second-order contributions for the special case of the $(4p_{3/2})^2-(4p_{3/2})^2[J=0]$ diagonal matrix element in two cases: (a) Coulomb-Coulomb diagram contributions and (b) Breit-Coulomb diagram contributions. The labels in Figs. 3(a) and

3(b) are the same as those used in Tables II and III. We can see from Fig. 3(a) that the R_1 diagram contribution is the largest for low-Z ions, while the V_1 diagram becomes dominant at high Z. The largest contributions of Breit-Coulomb type arise from the diagram BV_3 [see Fig. 3(b)].

For each of the second-order matrix elements, the Z dependence of each contributing diagram is smooth. Moreover, the leading term in a power series in Z for the second-order Coulomb-Coulomb energy is a constant. We may write

$$E^{(2)} = E_{20} + E_{22}(\alpha Z)^2 + E_{24}(\alpha Z)^4 + \cdots + \frac{1}{Z}[E'_{30} + E'_{32}(\alpha Z)^2 + E'_{34}(\alpha Z)^4 + \cdots] + \cdots . \quad (2)$$

The $1/Z$ terms in Eq. (2) describe the deviation from constancy in the DF case which is obvious for $Z<40$ from Fig. 3(a). The leading term in Z for the second-order Breit-Coulomb contributions is $(\alpha Z)^2$. The corresponding expansion in powers of Z is

$$B^{(2)} = (\alpha Z)^2 \left\{ B_{20} + B_{22}(\alpha Z)^2 + B_{24}(\alpha Z)^4 + \cdots + \frac{1}{Z}[B'_{30} + B'_{32}(\alpha Z)^2 + B'_{34}(\alpha Z)^4 + \cdots] + \cdots \right\}. \quad (3)$$

The curves for $E^{(2)}$ shown in Fig. 3(a) change by less than a factor of 2 over the range $Z=40-100$. The same is true of $B^{(2)}$, provided we divide out the factor $(\alpha Z)^2$.

C. Diagonalization and QED effects

The matrix elements presented so far represent the second-order matrix elements of the effective model-space Hamiltonian, Eq. (1), before diagonalization within the model space. To determine the first-order energies of the states under consideration, we diagonalize the (symmetric) first-order effective Hamiltonian, including both the Coulomb and Breit interactions. The second-order Coulomb corrections were determined by solving the nonsymmetric eigenvalue equation

$$H^{\text{eff}}C = EC, \quad (4)$$

with the first- plus second-order effective Hamiltonian. Terms of first and second order in the Coulomb interaction, and up to first-order in the Breit interaction, are included in H^{eff}. The resulting eigenvectors are used to determine the second-order Breit correction and the QED correction. The difference between the energies obtained using the first- plus second-order Hamiltonian and those determined using only the first-order Hamiltonian give the second-order energies.

To determine QED corrections for Zn-like ions, one can in principle use a generalization of the *ab initio* screened QED method of Blundell [24] for Cu-like ions, which consist of a single valence electron outside a Ni-like core. In those calculations, the self-energy and vacuum polarization of the valence state were calculated in the sum of the nuclear potential and Hartree potential of the core, thus accounting nonperturbatively for the bulk of the screening effect of the core electrons. Further small screening contributions were then added perturbatively corresponding to the exchange (as opposed to direct) interaction between the valence electron and the core and to the relaxation of the core in the presence of the valence electron. A similar approach was presented recently for Cu-like ions by Chen *et al.* [25] in which the exchange potential was treated via a local-density Slater-type potential. Now, in setting up a QED calculation for Zn-like ions, just as in RMBPT, it is natural to start from a suitable V^{N-2} potential for the closed-shell Ni-like core. A subset of the QED perturbation terms for Zn-like ions are then identical to those discussed above that have already been calculated for the Cu-like ions, where the potential was also taken to be that of the Ni-like core. Treating these terms as an effective interaction within RMBPT, one finds that they all correspond to one-body operators, analogous to the RMBPT diagrams in Fig. 1. Accordingly, they contribute terms of the form $\delta_{vv'}\delta_{ww'}(\delta\epsilon_v + \delta\epsilon_w)$ to the *diagonal* of the effective Hamiltonian (1), where $\delta\epsilon_v$ is the screened QED shift of a valence electron v for a Cu-like ion. The model-space Hamiltonian should then be rediagonalized. As mentioned above, we treat the QED perturbatively within the model space by using the eigenvectors determined by diagonalizing H^{eff} through second order.

A full treatment of QED in Zn-like ions will also bring in the screening effect of the two valence electrons on each other. These QED diagrams are similar to those describing the core relaxation in Ref. [24], but with the core electron replaced by the other valence electron. Treated as effective interactions within RMBPT, such diagrams correspond to two-body operators, analogous to the RMBPT diagrams in Fig. 2, and contribute to both the diagonal and off-diagonal terms of the effective Hamiltonian. We have estimated these contributions, finding them to be small, at the 0.01 eV level for $Z=74$. This is of the order of the experimental error, as well as at the expected level of further omitted QED effects (such as the frequency-dependent and negative-energy contributions of the RMBPT terms), and we omit them here. Note that the dominant effect of the two valence electrons in a Zn-like ion arises from the one-body QED terms, coupled with the fact that the physical states are now linear combinations of jj-coupled states, as discussed in the previous paragraph.

When *ab initio* QED calculations for Cu-like ions are available, we use them (in particular, for the $4s^2\ ^1S_0 - 4s4p\ ^1P_1$ transition). In other cases, the QED contributions can be determined approximately using the one-electron hydrogenic Lamb shift data given in Refs. [27–30] with $Z \rightarrow Z-12$ for $4lj$ states. To check the accuracy of this approach, in Table IV we compare our one-electron QED corrections thus calculated with the *ab initio* results of Blundell [24] and Chen *et al.* [25] for Cu-like ions. We can see that the disagreement between our phenomenological values for one-electron QED and results from Refs. [24,25] is about 2%.

The first- and second-order energies are shown graphically in Figs. 4 and 5 and listed in Table V. In Fig. 4, we show the Z dependence of the second-order Coulomb-Coulomb contributions $E^{(2)}$ for five states. We can see from Fig. 4 that the absolute value of $E^{(2)}$ slowly increases with Z.

The variation with Z of the second-order Coulomb energy $E^{(2)}$, the first- and second-order Breit energies $B^{(1)}$ and $B^{(2)}$,

TABLE IV. QED corrections (eV) for Cu-like ions. Present results (a) given by a phenomenological approach (see text) are compared with *ab initio* results of (b) Blundell [24] and (c) Chen *et al.* [25].

	$4s-4p_{1/2}$			$4s-4p_{3/2}$			$4p_{1/2}-4d_{3/2}$	
Z	(a)	(b)	(c)	(a)	(b)	(c)	(a)	(c)
70	−1.09	−1.06	−1.08	−1.00	−0.96	−0.98	−0.08	−0.07
74	−1.37	−1.34	−1.36	−1.26	−1.22	−1.24	−0.12	−0.11
76	−1.53	−1.50[a]	−1.52	−1.41	−1.36[a]	−1.39	−0.15	−0.13
79	−1.81	−1.76[a]	−1.78	−1.65	−1.60[a]	−1.63	−0.20	−0.18
82	−2.11	−2.05	−2.07	−1.93	−1.88	−1.91	−0.26	−0.24
83	−2.22	−2.15	−2.17	−2.04	−1.98	−2.01	−0.29	−0.27
90	−3.13	−2.98	−3.00	−2.87	−2.78	−2.82	−0.52	−0.49
92	−3.44	−3.25	−3.27	−3.15	−3.05	−3.09	−0.61	−0.58

[a]Calculated for this work using the method of Ref. [24].

and the QED contributions E_{LS} is illustrated in Fig. 5. Data for $(4p^2)^1S_0$ and $(4s^2)^1S_0$ states, respectively, are given in the two panels of Fig. 5. We can see that $E^{(2)}$ is dominant up to $Z=74$ for the $(4p^2)^1S_0$ and $(4s^2)^1S_0$ states. The QED contribution E_{LS} is smaller than all other contributions to the $(4p^2)^1S_0$ energy for all Z. The situation is somewhat different for the $(4s^2)^1S_0$ state where the curve E_{LS} crosses $B^{(2)}$ first for $Z>37$, then crosses the $E^{(2)}$ curve for $Z>73$, and for higher Z is smaller than the $B^{(1)}$ values.

In Table V, we list the energies of the 44 even-parity and 40 odd-parity levels in Zn-like xenon ($Z=54$). We tabulate the following separate contributions: zeroth- plus first-order energy $E^{(0+1)}\equiv E^{(0)}+E^{(1)}+B^{(1)}$, second-order Coulomb energy $E^{(2)}$, second-order Breit-Coulomb correction $B^{(2)}$, QED correction E_{LS}, and total theoretical energy E_{tot}. Both *jj*- and *LS*-coupling designations are used in Table V. As can be seen from Table V, the values of the second-order contributions $E^{(2)}$ and $B^{(2)}$ do not change very much inside complexes of states with given J; however, the QED contributions E_{LS} differ by two to three orders of magnitude. The ratio of the second-order Breit-Coulomb correction $B^{(2)}$ and Coulomb energy $E^{(2)}$ is about 1/10, and the ratio of $E^{(2)}$ and $E^{(0+1)}$ is about 1/300.

Energies, relative to the ground state, of odd- and even-parity states with $J=0-3$, divided by $(Z-21)^2$, are shown in Fig. 6. It should be noted that Z was decreased by 21 to provide a better presentation of the energy plots. As in Table V, we use both *jj*- and *LS*-coupling designations. We plot the limited number of energy levels to illustrate the change of mixing of levels belonging to different configurations with

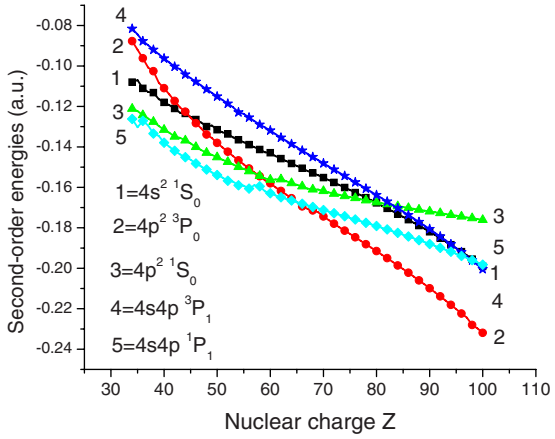

FIG. 4. (Color online) Second-order Coulomb energies after diagonalization are shown as a function of nuclear charge Z.

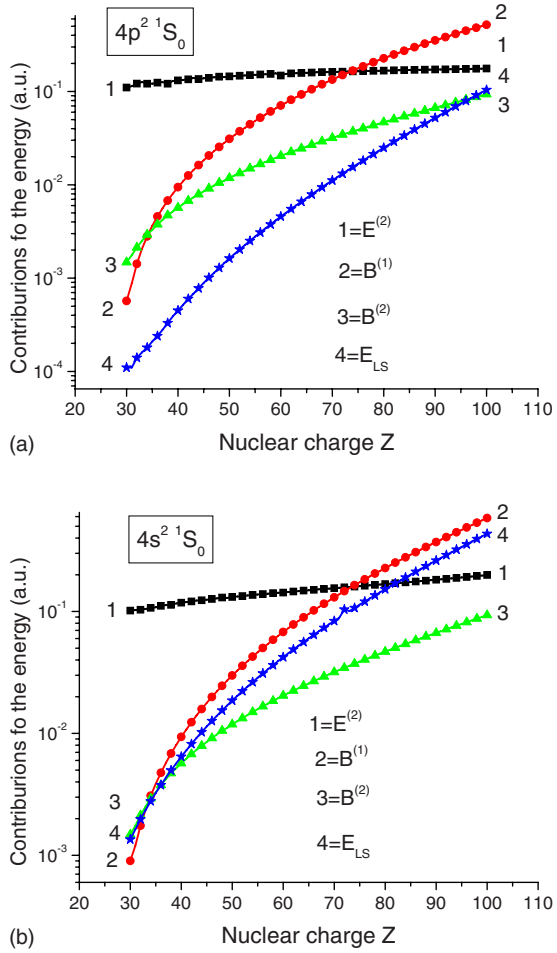

FIG. 5. (Color online) Contributions to the energies of the $(4p^2)^1S_0$ and $(4s^2)^1S_0$ states as a function of nuclear charge Z.

TABLE V. Energies of Zn-like xenon, $Z=54$. Notation: $E^{(0+1)}=E^{(0)}+E^{(1)}+B^{(1)}$, $E_{\rm tot}=E^{(0+1)}+E^{(2)}+B^{(2)}+E_{\rm LS}$.

jj-label	LSJ	$E^{(0+1)}$	$E^{(2)}$	$B^{(2)}$	$E_{\rm LS}$	$E_{\rm tot}$	jj-label	LSJ	$E^{(0+1)}$	$E^{(2)}$	$B^{(2)}$	$E_{\rm LS}$	$E_{\rm tot}$
$4s_{1/2}4s_{1/2}$	$^1S_0$	−13511671	−30065	−3289	5796	−13539229	$4s_{1/2}4p_{1/2}$	$^3P_0$	−13140633	−25693	−3405	2948	−13166783
$4p_{1/2}4p_{1/2}$	$^3P_0$	−12646972	−32238	−3609	77	−12682742	$4p_{3/2}4d_{3/2}$	$^3P_0$	−11675706	−30527	−3479	215	−11709498
$4p_{3/2}4p_{3/2}$	$^1S_0$	−12319340	−32883	−3464	546	−12355141	$4d_{5/2}4f_{5/2}$	$^3P_0$	−10152544	−34304	−2816	32	−10189632
$4d_{3/2}4d_{3/2}$	$^3P_0$	−10950854	−33470	−3562	−70	−10987955							
$4d_{5/2}4d_{5/2}$	$^1S_0$	−10847155	−38502	−3581	93	−10889145	$4s_{1/2}4p_{1/2}$	$^3P_1$	−13115850	−27091	−3427	2962	−13143406
$4f_{5/2}4f_{5/2}$	$^3P_0$	−9394210	−33710	−2066	−15	−9430001	$4s_{1/2}4p_{3/2}$	$^1P_1$	−12896460	−34923	−3408	3146	−12931645
$4f_{7/2}4f_{7/2}$	$^1S_0$	−9319922	−42509	−2156	15	−9364572	$4p_{1/2}4d_{3/2}$	$^3D_1$	−11789606	−34763	−3597	−8	−11827975
							$4p_{3/2}4d_{3/2}$	$^3P_1$	−11671056	−31134	−3475	220	−11705444
$4s_{1/2}4d_{3/2}$	$^3D_1$	−12531305	−29570	−3488	288	−12564076	$4p_{3/2}4d_{5/2}$	$^1P_1$	−11577394	−37148	−3523	322	−11617742
$4p_{1/2}4p_{3/2}$	$^3P_1$	−12265732	−30605	−3407	2871	−12296872	$4d_{3/2}4f_{5/2}$	$^3D_1$	−10171026	−34289	−2790	−40	−10208145
$4p_{3/2}4f_{5/2}$	$^3D_1$	−10937322	−32693	−3530	9	−10973537	$4d_{5/2}4f_{5/2}$	$^3P_1$	−10152632	−34275	−2797	34	−10189671
$4d_{3/2}4d_{5/2}$	$^3P_1$	−10883941	−33013	−2753	239	−10919468	$4d_{5/2}4f_{7/2}$	$^1P_1$	−10085007	−42449	−2840	54	−10130241
$4f_{5/2}4f_{7/2}$	$^3P_1$	−9393494	−33563	−2052	−1	−9429110							
							$4s_{1/2}4p_{3/2}$	$^3P_2$	−12997554	−24507	−3306	3185	−13022181
$4s_{1/2}4d_{3/2}$	$^1D_2$	−12526850	−27902	−3478	409	−12557821	$4s_{1/2}4f_{5/2}$	$^3F_2$	−11873828	−26011	−3518	−9	−11903366
$4s_{1/2}4d_{5/2}$	$^3D_2$	−12392392	−26793	−3383	678	−12421889	$4p_{1/2}4d_{3/2}$	$^1D_2$	−11799040	−30628	−3528	92	−11833103
$4p_{1/2}4p_{3/2}$	$^3P_2$	−12256264	−30698	−3399	2887	−12287473	$4p_{1/2}4d_{5/2}$	$^3F_2$	−11699060	−28599	−3449	242	−11730866
$4p_{3/2}4p_{3/2}$	$^1D_2$	−12158522	−38576	−3455	2678	−12197875	$4p_{3/2}4d_{3/2}$	$^3D_2$	−11656870	−30635	−3447	296	−11690657
$4p_{1/2}4f_{5/2}$	$^3F_2$	−11057928	−28833	−2980	−17	−11089758	$4p_{3/2}4d_{5/2}$	$^3P_2$	−11475392	−32520	−2681	2872	−11507721
$4p_{3/2}4f_{5/2}$	$^3D_2$	−10973165	−33116	−3376	−30	−11009686	$4d_{3/2}4f_{5/2}$	$^3F_2$	−10235896	−29183	−2771	−66	−10267915
$4p_{3/2}4f_{7/2}$	$^1D_2$	−10959132	−31286	−3344	38	−10993724	$4d_{3/2}4f_{7/2}$	$^1D_2$	−10202411	−30463	−2735	24	−10235586
$4d_{3/2}4d_{3/2}$	$^3F_2$	−10920900	−31934	−3440	102	−10956172	$4d_{5/2}4f_{5/2}$	$^3D_2$	−10171908	−33980	−2779	7	−10208659
$4d_{5/2}4d_{5/2}$	$^3P_2$	−10887364	−32929	−2783	233	−10922842	$4d_{5/2}4f_{7/2}$	$^3P_2$	−10153455	−34089	−2768	51	−10190261
$4d_{3/2}4d_{5/2}$	$^1D_2$	−10818869	−41960	−2978	244	−10863563							
$4f_{5/2}4f_{5/2}$	$^3F_2$	−9434878	−30916	−2040	−32	−9467865	$4s_{1/2}4f_{5/2}$	$^3F_3$	−11814654	−27024	−3485	136	−11845026
$4f_{5/2}4f_{7/2}$	$^1D_2$	−9402855	−34864	−2043	2	−9439761	$4s_{1/2}4f_{7/2}$	$^1F_3$	−11676200	−31069	−3435	327	−11710377
$4f_{7/2}4f_{7/2}$	$^3P_2$	−9392174	−33408	−1995	28	−9427548	$4p_{1/2}4d_{5/2}$	$^3F_3$	−11621753	−31875	−3340	646	−11656322
							$4p_{3/2}4d_{3/2}$	$^3D_3$	−11473127	−32576	−2652	2885	−11505471
$4s_{1/2}4d_{5/2}$	$^3D_3$	−12237979	−30216	−3373	2980	−12268587	$4p_{3/2}4d_{5/2}$	$^1F_3$	−11400271	−42726	−2872	2472	−11443397
$4p_{1/2}4f_{5/2}$	$^3F_3$	−11063092	−31087	−2803	−2	−11096984	$4d_{3/2}4f_{5/2}$	$^3F_3$	−10227665	−28968	−2726	−7	−10259367
$4p_{1/2}4f_{7/2}$	$^1F_3$	−11049842	−30248	−2803	55	−11082838	$4d_{3/2}4f_{7/2}$	$^3G_3$	−10184046	−35170	−2825	−65	−10222106
$4p_{3/2}4f_{5/2}$	$^3G_3$	−10973122	−30223	−3302	49	−11006599	$4d_{5/2}4f_{5/2}$	$^3D_3$	−10162161	−34738	−2781	18	−10199663
$4p_{3/2}4f_{7/2}$	$^3D_3$	−10915648	−30505	−2743	243	−10948653	$4d_{5/2}4f_{7/2}$	$^1F_3$	−10134042	−39230	−2785	75	−10175983
$4d_{3/2}4d_{5/2}$	$^3F_3$	−10889706	−32811	−2794	242	−10925069							
$4f_{5/2}4f_{7/2}$	$^3F_3$	−9433122	−30734	−2002	−1	−9465859	$4s_{1/2}4f_{7/2}$	$^3F_4$	−11709105	−23631	−3380	374	−11735742
							$4p_{3/2}4d_{5/2}$	$^3F_4$	−11469943	−32663	−2620	2901	−11502324
$4p_{1/2}4f_{7/2}$	$^3F_4$	−11063724	−28330	−2859	45	−11094868	$4d_{3/2}4f_{5/2}$	$^1G_4$	−10257408	−27780	−2737	−78	−10288004
$4p_{3/2}4f_{5/2}$	$^1G_4$	−10977282	−26166	−3096	148	−11006395	$4d_{3/2}4f_{7/2}$	$^3H_4$	−10240599	−27686	−2704	−3	−10270993
$4p_{3/2}4f_{7/2}$	$^3G_4$	−10959128	−29780	−3186	124	−10991970	$4d_{5/2}4f_{5/2}$	$^3F_4$	−10214763	−28194	−2681	78	−10245559
$4d_{3/2}4d_{5/2}$	$^3F_4$	−10892117	−33450	−2925	216	−10928277	$4d_{5/2}4f_{7/2}$	$^3G_4$	−10170786	−34142	−2777	18	−10207686
$4d_{5/2}4d_{5/2}$	$^1G_4$	−10789403	−48963	−3110	172	−10841304							
$4f_{5/2}4f_{5/2}$	$^3H_4$	−9447725	−30804	−2029	−46	−9480604	$4d_{3/2}4f_{7/2}$	$^3H_5$	−10242201	−27756	−2690	−2	−10272649
$4f_{5/2}4f_{7/2}$	$^3F_4$	−9432277	−30859	−1990	−1	−9465128	$4d_{5/2}4f_{5/2}$	$^3G_5$	−10161826	−34269	−2730	66	−10198760
$4f_{7/2}4f_{7/2}$	$^1G_4$	−9427465	−30834	−1948	46	−9460201	$4d_{5/2}4f_{7/2}$	$^1H_5$	−10088749	−49263	−2809	29	−10140792
							$4d_{5/2}4f_{7/2}$	$^3H_6$	−10225302	−27243	−2648	86	−10255107
$4p_{3/2}4f_{7/2}$	$^3G_5$	−10911503	−30844	−2635	290	−10944690							
$4f_{5/2}4f_{7/2}$	$^3H_5$	−9444912	−30584	−1974	−1	−9477471							
$4f_{5/2}4f_{7/2}$	$^3H_6$	−9441864	−30385	−1912	44	−9474117							
$4f_{7/2}4f_{7/2}$	$^1I_6$	−9400377	−40584	−1957	9	−9442909							

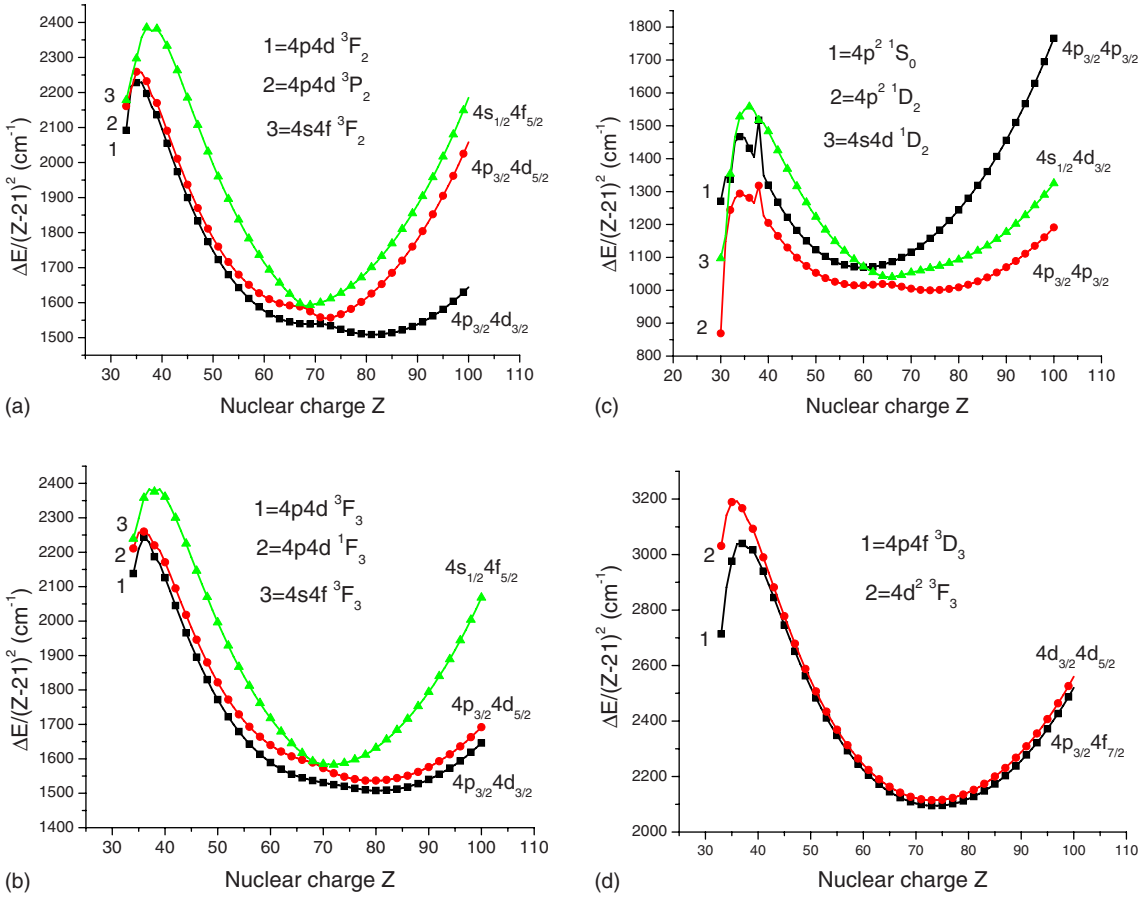

FIG. 6. (Color online) Excitation energies $\Delta E/(Z-21)^2$ in cm^{-1} for Zn-like ions as a function of Z.

change of Z. We can observe such mixing for the levels of odd-parity complexes with $J=2$ and $J=3$ (top panels of Fig. 6) and even-parity complexes with $J=2$ (left-bottom panel of Fig. 6) in the range $Z=65-68$. The curve for the energy of the $4p4d\ ^1F_3$ level almost crosses the curve for the $4s4f\ ^3F_3$ level. The difference of energies between the two levels is equal to 8800 cm^{-1} at $Z=68$ (about 0.25% from the energy of these levels). We can see a similar behavior of the curves for the $4p4d\ ^3P_2$ and $4s4f\ ^3F_2$ levels and the $4p^2\ ^1D_2$ and $4s4d\ ^1D_2$ levels.

It is known that the crossing of energy levels inside a complex with fixed J is forbidden by the Wigner and Neumann theorem (see, for example, Ref. [31]). We can observe from the top-right panel of Fig. 6 that the curves describing the energy of the $4p4d\ ^1F_3$ and $4s4f\ ^3F_3$ levels do not cross at $Z=68$ and that curve "3" stays above curve "2" for the entire range $Z=32-100$. A similar behavior for the curves describing the energy of the $4p4d\ ^3P_2$ and $4s4f\ ^3F_2$ levels (top-left panel of Fig. 6) and of the $4p^2\ ^1D_2$ and $4s4d\ ^1D_2$ levels (bottom-left panel of Fig. 6) may also be observed. Additionally, it should be noted that the curves describing the energy of the $4p4f\ ^3D_3$ and $4d^2\ ^3F_3$ levels (bottom-right panel of Fig. 6) are almost coincident with one another. The difference in energies between the two levels is about 1% for entire Z interval.

It should be noted that the LS designations were chosen based upon small values of the multiplet splitting for low-Z ions. To confirm those LS designations, we obtained the fine-structure splitting for the even-parity $4s4d\ ^3D$, $4p^2\ ^3P$, $4d^2[^3P,^3F]$, $4p4f[^3D,^3F,^3G]$, and $4f^2[^3P,^3F,^3H]$ states and odd-parity $4s4p\ ^3P$, $4s4f\ ^3F$, $4p4d[^3P,^3D,^3F]$, and $4d4f[^3P,^3D,^3F,^3G,^3H]$ states.

The energy differences between levels of even- and odd-parity triplet terms, divided by $(Z-21)^2$, are illustrated in Figs. 7 and 8, respectively. The energy intervals for the $4p^2(^3P_2\text{-}^3P_1)$, $4d^2(^3F_4\text{-}^3F_3)$, $4s4p(^3P_1\text{-}^3P_0)$, $4p4d(^3P_1\text{-}^3P_0)$, and $4p4d(^3D_3\text{-}^3D_2)$ states are very small and almost do not change with Z, as can be seen from Figs. 7 and 8. There is a very sharp change of splitting around $Z=70$ for the $4p4d(^3P_2\text{-}^3P_1)$ terms, but the energies $\Delta E/(Z-21)^2$ change by only a small amount, from -10 cm^{-1} to 35 cm^{-1}. The energy intervals vary strongly with Z for the $4p^2(^3P_1\text{-}^3P_0)$ and $4s4p(^3P_2\text{-}^3P_1)$ intervals. The triplet splitting for the $4s4d\ ^3D$, $4d^2[^3P,^3F]$, $4p4f[^3D,^3F,^3G]$, $4s4f\ ^3F$, $4p4d[^3P,^3D,^3F]$, and $4d4f[^3P,^3D,^3F,^3G,^3H]$ terms change in the small interval of 50–150 in units of $(Z-21)^2$ cm^{-1}, which amounts to 2%–5% of the energy of those terms. Our calculations show that the fine structures of almost all the levels illustrated in Figs. 7 and 8 do not follow the Landé rules even for small Z. The unusual splitting may be caused by changes from LS to jj coupling, with mixing from other triplet and singlet states. The different J states are mixed differently. Further experimental confirmation would

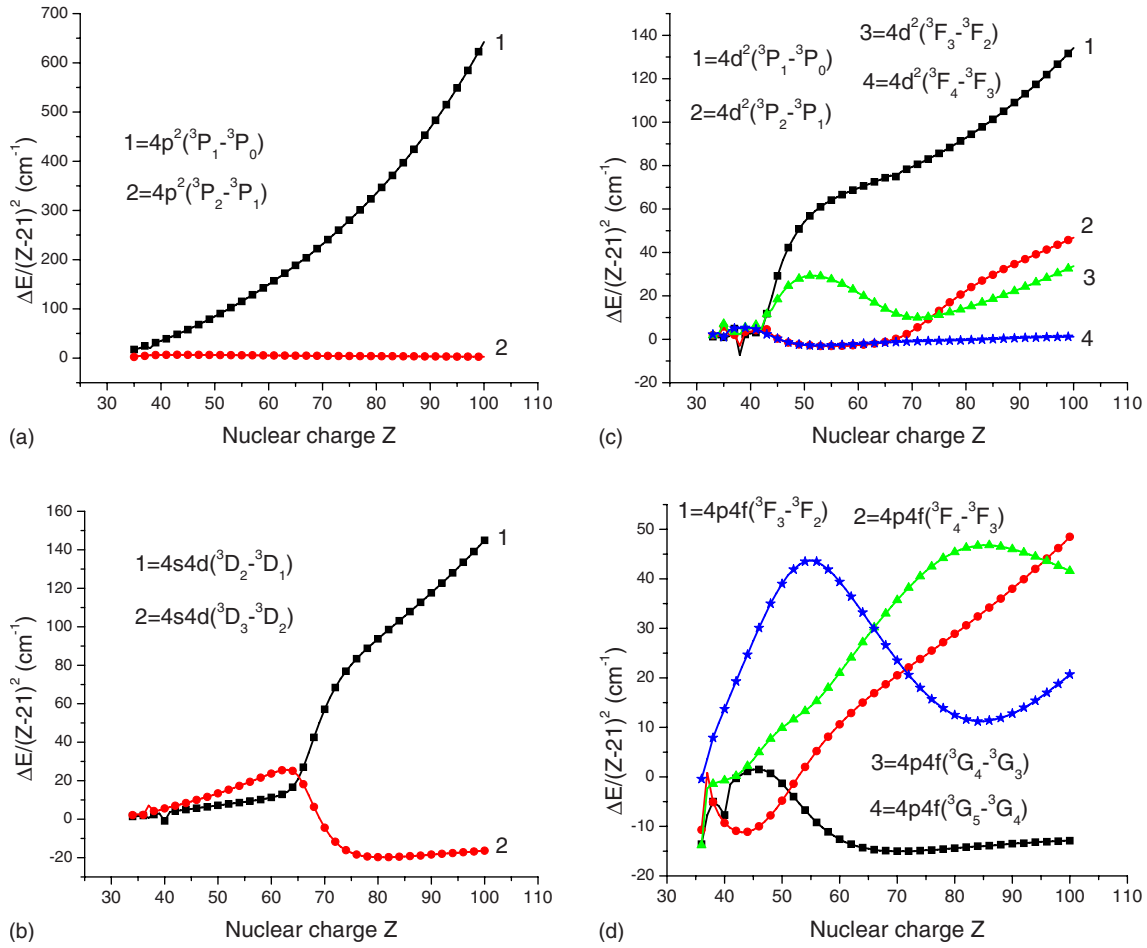

FIG. 7. (Color online) Energy splitting $\Delta E/(Z-21)^{-2}$ in cm^{-1} for terms of even-parity states for Zn-like ions as a function of Z.

be very helpful in verifying the correctness of these sometimes sensitive mixing parameters.

III. BREIT INTERACTION

The first-order Breit and second-order Breit-Coulomb contributions $B^{(1)}$ and $B^{(2)}$ discussed above are obtained from the $E^{(1)}$ and $E^{(2)}$ Coulomb expressions by changing $g_{ijkl} \rightarrow g_{ijkl}+b_{ijkl}$ and keeping only terms that are linear in b_{ijkl}. Here g_{ijkl} is the Coulomb matrix element. The term b_{ijkl} is a two-particle matrix element of the Breit interaction [32]

$$B = -\frac{\alpha}{r_{12}}\left\{\boldsymbol{\alpha}_1 \cdot \boldsymbol{\alpha}_2 - \frac{1}{2}[\boldsymbol{\alpha}_1 \cdot \boldsymbol{\alpha}_2 - (\boldsymbol{\alpha}_1 \cdot \hat{\mathbf{r}}_{12})(\boldsymbol{\alpha}_2 \cdot \hat{\mathbf{r}}_{12})]\right\}, \tag{5}$$

where $\boldsymbol{\alpha}_1$ is a Dirac matrix, $\hat{\mathbf{r}}_{12}=\mathbf{r}_{12}/r_{12}$, and α is the fine structure constant.

In this perturbative treatment of the Breit interaction, we omit Breit contributions to the Dirac-Fock potential and evaluate Coulomb and Breit-Coulomb corrections through second order. This is the approach that was used in the previous section. In an alternative approach, to be considered in this section, we include both Coulomb and Breit contributions to the Dirac-Fock potential (giving the Breit-Dirac-Fock potential) and then treat the *residual* Breit and Coulomb interactions perturbatively. The details of such a treatment were discussed recently by Derevianko [33], Kreuter *et al.* [34], and Dzuba *et al.* [35].

Similar to the Coulomb interaction $1/r_{12}$, inclusion of the Breit interaction B creates a self-consistent Breit-Dirac-Fock (BDF) potential. This requires developing a new code for the DF functions: Breit-Dirac-Hartree-Fock (BDHF) to replace our Dirac-Hartree-Fock (DFH) code. The difference in the DF one-electron energies $\Delta E(nl)$ calculated by the DHF and BDHF codes as functions of nuclear charge Z is illustrated in Fig. 9. The difference between $E^{\mathrm{DF}}(nl)$ calculated by the two codes is positive for the $4s_{1/2}$, $4p_j$, and $4d_j$ states for the entire Z interval; however, it becomes negative for the $4f_j$ states for low-Z ions. The changes of sign in $\Delta E(4f_j)$ lead to the sharp feature on the curves describing the Z dependence of $\Delta E(4f_j)$ values seen in Fig. 9. The values of $\Delta E(4f_j)$ increase with Z as $(Z-c)^3$ with the screening correction $c=21$.

To calculate the correction to the energy matrix elements arising from the Breit interaction, we modified the generation of the B-spline basis set to intrinsically include the Breit interaction on the same footing as the Coulomb interaction. Once this is done, the one-potential operator, represented in Figs. 1 and 2 by a solid circle, vanishes identically. This is

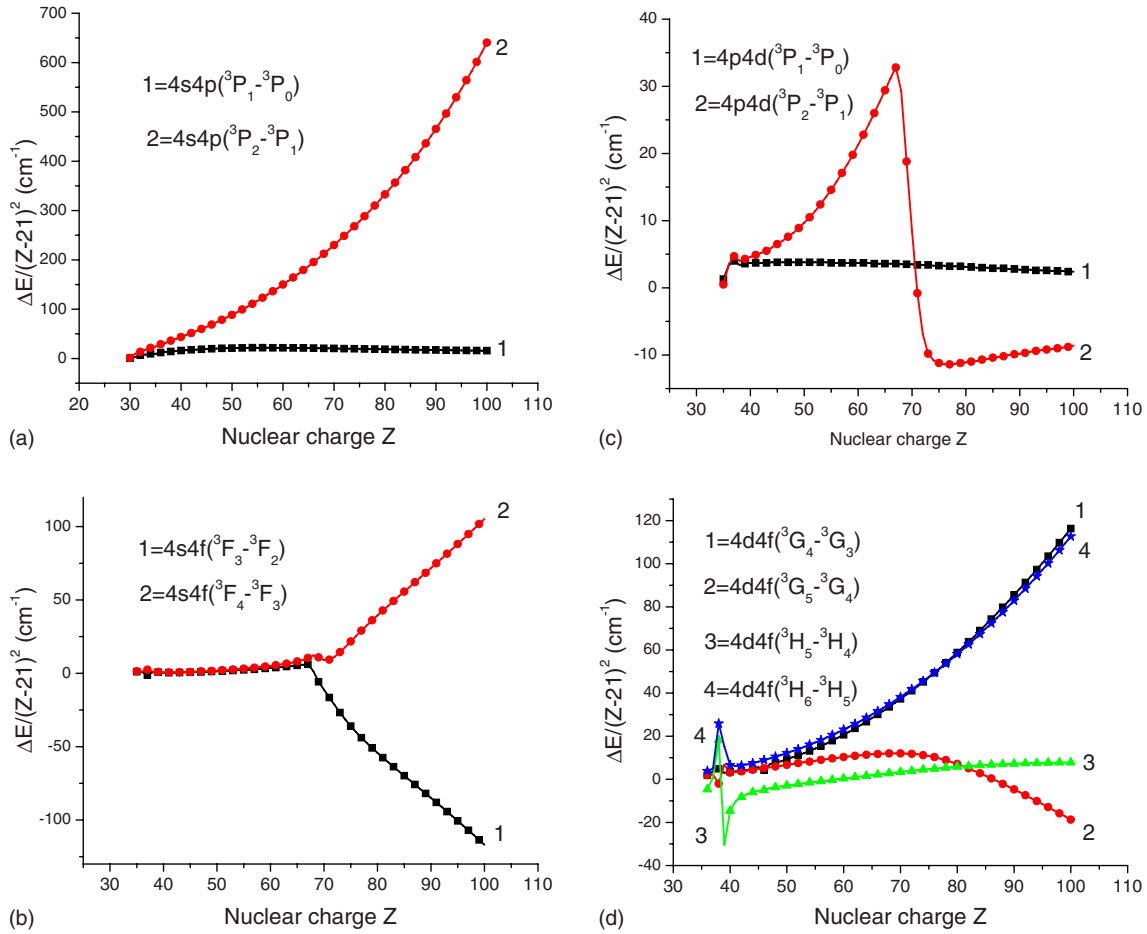

FIG. 8. (Color online) Energy splitting $\Delta E/(Z-21)^{-2}$ in cm^{-1} for terms of odd-parity states for Zn-like ions as a function of Z.

analogous to the way that in nonrelativistic MBPT the corresponding one-potential operator vanishes when expanding perturbatively around the HF potential. Thus, the contributions BV_3 and BR_4 now vanish identically. Otherwise, the remaining contributions given in Tables II and III do not change very much; the difference in new values is about 0.01%–0.1%. Additionally, we need to remove the one-potential valence contribution from a first-order Breit correction, since that contribution was already incorporated in new DF energies.

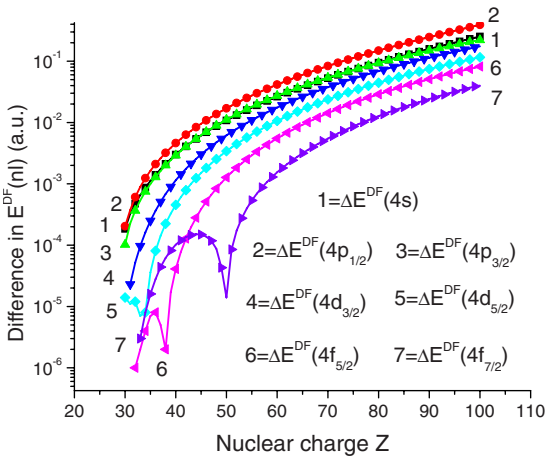

FIG. 9. (Color online) The difference in the one-electron energies $\Delta E(nl)$ in a.u. for the Breit-Dirac-Fock (BDF) and Dirac-Fock (DF) potentials as a function of nuclear charge Z.

In Fig. 10, we illustrate the difference in the first-order Breit term $B^{(1)}$ and second-order Breit-Coulomb term $B^{(2)}$ calculated by using the DF and BDF potentials as functions of nuclear charge Z. It should be noted that the values of those differences for the first-order Breit contribution $\Delta B^{(1)}(4l4l'\ ^{1,3}L_J)$ are positive for the entire interval of Z. However, the values of the differences for the second-order Breit-Coulomb contribution $\Delta B^{(2)}(4l4l'\ ^{1,3}L_J)$ are negative. We can see from Fig. 10 that the values of $\Delta B^{(1)}(4l4l'\ ^{1,3}L_J)$ and $\Delta B^{(2)}(4l4l'\ ^{1,3}L_J)$ increase by three to four orders of magnitude when Z increases from $Z=30$ up to $Z=100$. Such a sharp increase is similar to the increase of the difference in one-electron eigenvalues $\Delta E(nl)$ for the DF and BDF potentials. We already mentioned that the values $\Delta E(4l)$ and $\Delta B^{(1)}(4l4l'\ ^{1,3}L_J)$ have a different sign and partly compensate each other. The $\Delta B^{(2)}(4l4l'\ ^{1,3}L_J)$ values are smaller than the $\Delta B^{(1)}(4l4l'\ ^{1,3}L_J)$ values by a factor of 10.

Now let us compare the two versions of RMBPT, based on the DF and BDF potential, respectively. As can be seen from Table VI, a small difference in final energies exists. In

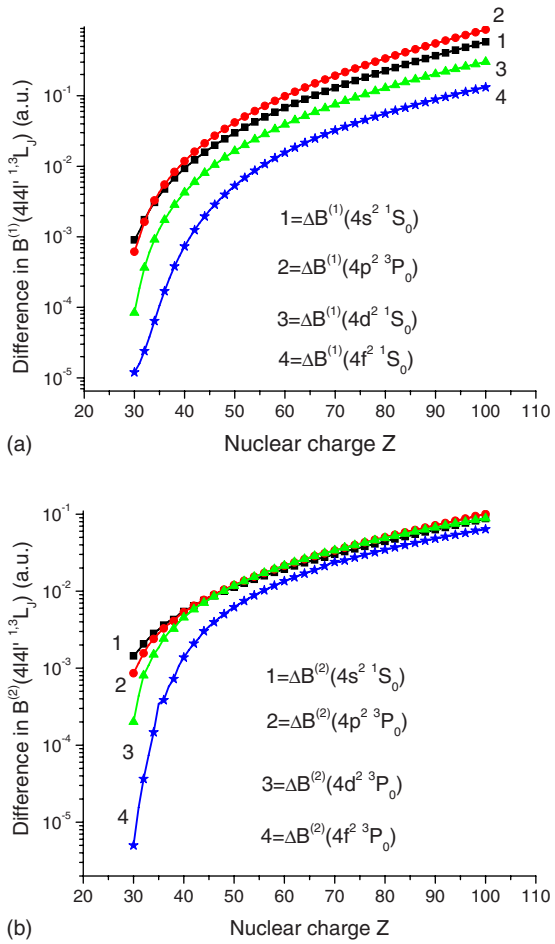

FIG. 10. (Color online) The difference in the first-order Breit term $B^{(1)}$ and second-order Breit-Coulomb term $B^{(2)}$ in a.u. calculated by using a Breit-Dirac-Fock (BDF) and Dirac-Fock (DF) potential as a function of the nuclear charge Z.

this table, we list the difference in energies of $4s^2\ ^1S_0$ and $4s4p\ ^{1,3}P_1$ states calculated using the BDF and DF potentials. The difference in the results obtained by two approaches increases slowly with Z from $Z=36$ up to $Z=92$.

In Table VII, we list energies of the $4s4p$ states given relative to the ground state for Zn-like ions with $Z=51-70$. Energies calculated by the BDF and DF versions of RMBPT are compared with experimental measurements given by Brown *et al.* [21]. We tabulate the following separate contributions: zeroth- plus first-order energy $E^{(0+1)}\equiv E^{(0)}+E^{(1)}+B^{(1)}$, second-order Coulomb energy $E^{(2)}$, second-order Breit-Coulomb correction $B^{(2)}$, QED correction E_{LS}, and total theoretical energy E_{tot}. The values of E_{tot} are compared with E_{expt}, and the difference $[E_{\mathrm{tot}}-E_{\mathrm{expt}}]$ is denoted by δE. We can see from this table that the value of δE is smaller for the results obtained by the BDF approach. We use this version of RMBPT in all results below.

Inasmuch as the one-body part of the Breit interaction, which as mentioned earlier dominates the second-order Coulomb-Breit energy, is included to all orders in the BDF wave function, we expect an RMBPT approach based on the BDF potential to be somewhat more accurate than one based on the DF potential. Indeed, our expectation is confirmed by the energy comparisons in Table VII. It should be noted that frequency-dependent corrections to the Breit interaction, which will lead to further small modifications of the theoretical energies, are omitted in the present calculations.

TABLE VI. The energy differences (cm^{-1}) in results calculated with a Breit-Dirac-Fock (BDF) potential and with a Dirac-Fock (DF) potential.

Z	$4s^2\ ^1S_0$	$4s4p\ ^3P_1$	$4s4p\ ^1P_1$
36	335	325	330
40	404	403	406
45	492	504	493
50	578	609	595
55	674	707	672
59	742	781	735
70	983	1059	990
74	1076	1159	1077
76	1124	1211	1121
79	1199	1290	1189
82	1278	1373	1260
83	1305	1401	1284
90	1508	1610	1458
92	1571	1674	1511

IV. COMPARISON OF RESULTS WITH OTHER THEORIES AND EXPERIMENTS

In Table VIII, we compare our RMBPT energies E_{tot} in Zn-like ions given relative to the ground state for ions with $Z=34-50$ with experimental data E_{expt} presented by Churilov *et al.* [11]. In this table, we present results for the 13 low-lying levels $4s4p[^1P_1,^3P_J]$, $4p^2[^1S_0,^3P_J,^1D_2]$, and $4s4d[^1D_2,^3D_J]$. We can see from Table VIII that the difference $\delta E=E_{\mathrm{tot}}-E_{\mathrm{expt}}$ decreases when Z increases; however, the value of δE for the $4s4d\ ^1D_2$ level is equal to $-1013\ \mathrm{cm}^{-1}$ for $Z=36$, $-196\ \mathrm{cm}^{-1}$ for $Z=42$, and $-1131\ \mathrm{cm}^{-1}$ for $Z=50$. Among the 13 levels listed in Table VIII, we find the smallest value of δE is for the $4p^2\ ^1D_2$ level: $8-253\ \mathrm{cm}^{-1}$. For the 11 ions listed in Table VIII, we find the best agreement between RMBPT and experimental values for Mo^{12+}; only for two levels is the value of δE about $700\ \mathrm{cm}^{-1}$. We cannot really explain why there is such a large deviation in values of δE from one ion to another. It was demonstrated previously (see Figs. 6–8) that the Z dependences of the energy levels are rather smooth curves.

RMBPT energies of the $4s4p\ ^1P_1$ level in Zn-like ions with $Z=70-92$ are compared in Table IX with experimental measurements E_{expt} given by Träbert *et al.* [17]. We tabulate the following separate contributions: zeroth- plus first-order energy $E^{(0+1)}\equiv E^{(0)}+E^{(1)}+B^{(1)}$, second-order Coulomb energy $E^{(2)}$, second-order Breit-Coulomb correction $B^{(2)}$, QED correction E_{LS}, and total theoretical energy E_{tot}. The values of E_{tot} are compared with E_{expt}, and the difference $[E_{\mathrm{tot}}-E_{\mathrm{expt}}]$ is denoted by δE. We can see from this table that the values of δE are smaller than any separate contributions,

TABLE VII. Energies (cm^{-1}) of the $4s4p$ states given relative to the ground state for Zn-like ions with $Z=51-70$. Notation: $E^{(0+1)}=E^{(0)}+E^{(1)}+B^{(1)}$, $\delta E=E_{tot}-E_{expt}$. Energy calculated with a Breit-Dirac-Fock (BDF) (RMBPT-b) and a Dirac-Fock (DF) (RMBPT-t) potential are compared with experimental measurements given by Brown *et al.* [21].

	$^3P_1$	$^1P_1$	$^3P_1$	$^1P_1$	$^3P_1$	$^1P_1$	$^3P_1$	$^1P_1$
	RMBPT-b		RMBPT-t		RMBPT-b		RMBPT-t	
	$Z=51$				$Z=52$			
$E^{(0+1)}$	346120	522904	346167	522959	362524	552456	362579	552515
$E^{(2)}$	3529	−4907	3509	−4914	3411	−5174	3304	−5057
$B^{(2)}$	−20	−30	−79	−93	−23	−34	−103	−118
E_{LS}	−2186	−2063	−2186	−2063	−2386	−2247	−2386	−2247
E_{tot}	347443	515904	347411	515888	363525	545001	363394	545093
E_{expt}	347441	516518	347441	516518	363533	545926	363533	545926
δE	2	−614	−30	−630	−8	−925	−139	−833
	$Z=53$				$Z=54$			
$E^{(0+1)}$	379071	583183	379135	583247	395747	615144	395821	615211
$E^{(2)}$	3295	−4810	3275	−4816	3365	−4655	2982	−4944
$B^{(2)}$	−25	−34	−107	−105	−26	−36	−137	−123
E_{LS}	−2598	−2442	−2598	−2442	−2822	−2647	−2822	−2647
E_{tot}	379743	575897	379705	575884	396264	607806	395844	607498
E_{expt}	379744	576442	379744	576442	396082	608280	396082	608280
δE	−1	−545	−39	−558	182	−474	−238	−782
	$Z=55$				$Z=57$			
$E^{(0+1)}$	412567	648429	412652	648500	446621	719268	446727	719346
$E^{(2)}$	3101	−4718	3086	−4708	2854	−4356	2829	−4123
$B^{(2)}$	−29	−39	−132	−118	−35	−43	−174	−91
E_{LS}	−3063	−2867	−3063	−2867	−3583	−3343	−3583	−3343
E_{tot}	412576	640805	412544	640807	445857	711526	445800	711789
E_{expt}	412558	641276	412558	641276	445831	711587	445831	711587
δE	18	−471	−14	−469	26	−61	−31	202
	$Z=60$				$Z=63$			
$E^{(0+1)}$	498782	837483	498926	837570	552299	972220	552485	972313
$E^{(2)}$	2480	−4356	2418	−4395	2228	−4098	2200	−4107
$B^{(2)}$	−45	−51	−204	−129	−54	−57	−272	−150
E_{LS}	−4478	−4161	−4478	−4161	−5524	−5117	−5524	−5117
E_{tot}	496739	828914	496663	828884	548948	962948	548889	962938
E_{expt}	496857	829208	496857	829208	548847	963094	548847	963094
δE	−118	−294	−194	−324	101	−146	42	−156
	$Z=64$				$Z=66$			
$E^{(0+1)}$	570455	1021264	570657	1021357	607303	1126222	607538	1126315
$E^{(2)}$	2132	−4017	2103	−4026	1955	−3839	1921	−3851
$B^{(2)}$	−57	−59	−293	−153	−64	−63	−337	−157
E_{LS}	−5909	−5469	−5909	−5469	−6736	−6226	−6736	−6226
E_{tot}	566621	1011720	566559	1011709	602457	1116095	602386	1116081
E_{expt}	566251	1011900	566251	1011900	602580	1113511	602580	1113511
δE	370	−180	308	−191	−123	2584	−194	2570
	$Z=68$				$Z=70$			
$E^{(0+1)}$	644852	1241061	645121	1241152	683119	1366744	683426	1366829
$E^{(2)}$	1703	−3738	1748	−3671	1590	−3504	1555	−3515
$B^{(2)}$	−72	−66	−384	−157	−80	−69	−429	−149
E_{LS}	−7646	−7057	−7646	−7057	−8644	−7971	−8644	−7971
E_{tot}	638836	1230200	638840	1230266	675984	1355200	675908	1355193
E_{expt}	639031	1229967	639031	1229967	674900	1355160	674900	1355160
δE	−195	233	−191	299	1084	40	1008	33

TABLE VIII. RMBPT energies E_{tot} of Zn-like ions given relative to the ground state for ions with $Z=34-50$ are compared with experimental data E_{expt} presented by Churilov *et al.* [11]. $\delta E=E_{tot}-E_{expt}$. Units: cm^{-1}.

	$4s4p$		$4s4p$		$4p^2$	$4p^2$	$4p^2$	$4p^2$	$4p^2$	$4s4d$		$4s4d$	
	$^3P_0$	$^3P_1$	$^3P_2$	$^1P_1$	$^3P_0$	$^3P_1$	$^3P_2$	$^1D_2$	$^1S_0$	$^3D_1$	$^3D_2$	$^3D_3$	$^1D_2$
							$Z=34$						
E_{tot}	90309	91935	95591	130757	211886	214207	214072	218701	247840	257924	258169	258532	278126
E_{expt}	89752	91335	94949	131733	211794	214089	213203	218618	248858	257533	257732	258066	279139
δE	557	600	642	−976	92	118	869	83	−1018	391	437	466	−1013
							$Z=36$						
E_{tot}	117590	120333	126864	170570	274833	279358	280299	288198	322193	350043	350463	350962	378620
E_{expt}	117390	120093	126553	170835	274932	279414	279715	288190	323036	349973	350417	351116	379488
δE	200	240	311	−265	−99	−56	584	8	−843	70	46	−154	−868
							$Z=41$						
E_{tot}	186540	193278	212309	271242	432259	447924	450556	473922	517355	580012	581540	584046	627075
E_{expt}	186370	193088	212044	271939	432669	448253	450414	473998	518094	580108	581633	584120	626459
δE	170	190	265	−698	−410	−329	142	−76	−739	−96	−93	−74	616
							$Z=42$						
E_{tot}	200431	208176	230919	292613	463986	483220	486135	513962	559022	626693	628549	631622	676368
E_{expt}	200311	207981	230639	293322	464442	483553	486037	514028	559817	626917	628737	631759	676564
δE	120	195	280	−709	−456	−333	98	−66	−795	−224	−188	−137	−196
							$Z=44$						
E_{tot}	228268	238199	269908	337000	527848	555758	559253	597631	646495	721401	724024	728475	777709
E_{expt}	228244	238118	269736	337727	528536	556205	559310	597781	646912	721791	724380	728801	778388
δE	24	81	172	−727	−688	−447	−57	−150	−417	−390	−356	−326	−679
							$Z=45$						
E_{tot}	242350	253494	290539	360296	559951	593211	597003	641572	691895	769691	772761	778045	829509
E_{expt}	242262	253346	290277	360610	560454	593613	596997	641627	692398	770097	773143	778260	830183
δE	88	148	262	−314	−504	−402	6	−55	−503	−406	−382	−215	−674
							$Z=46$						
E_{tot}	256487	268867	311904	384093	592223	631492	635578	686990	738936	818629	822193	828418	882087
E_{expt}	256490	268745	311648	384718	592868	631937	635575	687168	739610	819163	822568	828773	882990
δE	−3	122	256	−625	−645	−445	3	−178	−674	−534	−375	−355	−903
							$Z=47$						
E_{tot}	270697	284365	334088	408696	624639	670669	675046	734016	787605	868301	872407	879689	935529
E_{expt}	270621	284251	333853	409312	625293	671127	675156	734179	787252	868764	872961	880128	936512
δE	76	114	235	−616	−654	−458	−110	−163	353	−463	−555	−439	−983
							$Z=48$						
E_{tot}	285138	300137	357296	434285	657271	710950	715618	782904	837988	918928	923625	932094	990073
E_{expt}	284831	299825	356855	434699	657783	711164	715502	782812	838635	919338	923991	932255	990770
δE	307	312	441	−415	−512	−214	116	92	−647	−410	−366	−161	−697
							$Z=49$						
E_{tot}	299088	315457	380861	460193	689781	751682	756638	833041	890436	969856	975197	984989	1045108
E_{expt}	299171	315385	380737	460878	690470	752160	756771	833140	890693	970737	976028	985393	1045944
δE	−83	72	124	−685	−689	−478	−133	−99	−257	−881	−831	−404	−837
							$Z=50$						
E_{tot}	313680	331455	405970	487609	722842	794051	799296	885669	944610	1022283	1028322	1039585	1101799
E_{expt}	313704	331470	405823	488338	723614	794616	799558	885922	945055	1023075	1029054	1040127	1102930
δE	−24	−15	147	−729	−772	−566	−263	−253	−445	−792	−732	−542	−1131

TABLE IX. Excitation energies of $4s4p\ ^1P_1$ levels in Zn-like ions. Experimental values E_{expt} are given by Träbert *et al.* [17]. Units: cm^{-1} .

	$Z=70$	$Z=74$	$Z=76$	$Z=79$
$E^{(0+1)}$	1366744	1655120	1820238	2097800
$E^{(2)}$	−3504	−3117	−2916	−2603
$B^{(2)}$	−69	−72	−72	−70
E_{LS}	−7971	−10070	−11264	−13250
E_{tot}	1355200	1641862	1805987	2081876
E_{expt}	1355160	1642036	1805576	2080806
δE	40	−174	411	1070
	$Z=82$	$Z=83$	$Z=90$	$Z=92$
$E^{(0+1)}$	2415825	2531800	3508421	3848972
$E^{(2)}$	−2275	−2162	−1301	−1029
$B^{(2)}$	−65	−63	−32	−18
E_{LS}	−15502	−16318	−23006	−25263
E_{tot}	2397983	2513258	3484082	3822662
E_{expt}	2397018	2511610	3480646	3818820
δE	965	1648	3436	3842

except the values of the second-order Breit-Coulomb contributions $B^{(2)}$. We obtain excellent agreement between our RMBPT values and experimental measurements; the δE values are 0.003%–0.1% of E_{expt}.

In Table X, we compare our RMBPT energies E_{tot} with recently published theoretical predictions E_{theo} made by Vilkas and Ishikawa [23] ($\delta E=E_{\text{tot}}-E_{\text{theo}}$). A relativistic MR-MP perturbation theory was used in Ref. [23]. Both *LS* and *jj* designations are used in Table X. Our *jj* designations are the same as those of Vilkas and Ishikawa [23], except for five cases where we use $4d_j4d_{j'}(J)$ designations instead of the $4p_j4f_{j'}(J)$ designations used in Ref. [23]. We demonstrated previously a large mixing between the $4p4f$ *LSJ* and $4d^2$ *LSJ* states (see the curves describing the energy of the $4p4f\ ^3D_3$ and $4d^2\ ^3F_3$ levels shown on bottom-right panel of Fig. 6). The strong mixing between the $4d_{3/2}4d_{5/2}(2)$ and $4d_{5/2}4d_{5/2}(2)$ states leads to interchanges between those states as Z varies (compare the fourth and fifth lines from the bottom of Table X). We can see from this table that the difference $\delta E=E_{\text{tot}}-E_{\text{theo}}$ is about 100–1000 cm^{-1} for most cases; however, there are some discrepancies that we cannot explain. The value $E=2\,674\,915\ \text{cm}^{-1}$ in the column with heading $Z=70$ appears twice in Table II of Ref. [23]. This value differs from our RMBPT values for the energy of the $4p_{3/2}4p_{3/2}(2)$ level by 978 cm^{-1}; however, the δE for the $4s_{1/2}4d_{5/2}(2)$ level is equal to 145 238 cm^{-1}. We think this was a misprint in Ref. [23], and we do not include this number in the column headed "δE" in Table X. Similar problems were found for the $4p_{3/2}4f_{7/2}(3)$ level with $Z=76$ (we do not include this in Table X).

TABLE X. RMBPT energies (E_{tot}) given relative to the ground state for ions with $Z=70$ and 92 are compared with the theoretical results of Vilkas and Ishikawa [23]. Units: cm^{-1}.

		$Z=70$		$Z=92$	
		E_{tot}	δE	E_{tot}	δE
$4s_{1/2}4p_{1/2}$	$^3P_0$	626926	−443	1053096	−1329
$4s_{1/2}4p_{1/2}$	$^3P_1$	675908	−320	1138177	−1105
$4s_{1/2}4p_{3/2}$	$^1P_1$	1355193	607	3822722	3528
$4s_{1/2}4p_{3/2}$	$^3P_2$	1228178	277	3641664	3030
$4p_{1/2}4d_{3/2}$	$^3D_1$	3175602	224	6734510	−60
$4p_{1/2}4d_{3/2}$	$^1D_2$	3247490	371	7177846	583
$4p_{3/2}4d_{3/2}$	$^3P_0$	3729898	873	9246895	4266
$4p_{3/2}4d_{3/2}$	$^3P_1$	3738223	912	9260385	4324
$4p_{3/2}4d_{5/2}$	$^1P_1$	3941327	1180	9888754	5344
$4p_{3/2}4d_{5/2}$	$^3P_2$	3832264	1067	9732479	4970
$4p_{1/2}4d_{5/2}$	$^3F_2$	3696247	854	7829066	3137
$4p_{1/2}4d_{5/2}$	$^3F_3$	3776341	1375	8031419	3601
$4p_{3/2}4d_{3/2}$	$^3D_2$	3758557	1246	9212337	4230
$4p_{3/2}4d_{3/2}$	$^3D_3$	3805414	1109	9272971	4319
$4p_{3/2}4d_{3/2}$	$^1F_3$	3973937	1246	9850742	5250
$4p_{3/2}4d_{5/2}$	$^3F_4$	3827296	1267	9667304	4779
$4s_{1/2}4f_{5/2}$	$^3F_2$	3053889	18	6546122	−474
$4s_{1/2}4f_{5/2}$	$^3F_3$	3244686	352	7185112	622
$4s_{1/2}4f_{7/2}$	$^1F_3$	3676406	907	7838749	3121
$4s_{1/2}4f_{7/2}$	$^3F_4$	3732084	1077	7980913	3635
$4p_{1/2}4p_{1/2}$	$^3P_0$	1432379	−339	2384828	−1958
$4p_{1/2}4p_{3/2}$	$^3P_1$	1988261	170	4899480	2227
$4p_{1/2}4p_{3/2}$	$^3P_2$	1999179	106	4915688	2175
$4p_{2/2}4p_{3/2}$	$^1S_0$	2678559	1109	7610621	6965
$4p_{3/2}4p_{3/2}$	$^1D_2$	2675893	978	7517442	6652
$4s_{1/2}4d_{3/2}$	$^3D_1$	2392629	393	5438127	773
$4s_{1/2}4d_{3/2}$	$^3D_2$	2413199	434	5491308	938
$4s_{1/2}4d_{5/2}$	$^1D_2$	2529677		6056852	1738
$4s_{1/2}4d_{5/2}$	$^3D_3$	2519173	611	5965995	1541
$4d_{3/2}4d_{3/2}$	$^3F_2$	5071288	1450	11625191	6004
$4d_{3/2}4d_{5/2}$	$^3P_1$	5090731	1628	11640414	6598
$4d_{3/2}4d_{5/2}$	$^3F_3$	5095503	1795	11752270	7016
$4d_{3/2}4d_{5/2}$	$^1D_2$	5193953	1482	12074529	
$4d_{5/2}4d_{5/2}$	$^3P_2$	5100002		11831974	6651
$4p_{3/2}4f_{7/2}$	$^3D_3$	5049989	1678	11589762	5881
$4p_{3/2}4f_{7/2}$	$^3G_4$	5023511	586	11670872	6403
$4p_{3/2}4f_{7/2}$	$^3G_5$	5080042	1759	11741171	6997

V. CONCLUSION

We have presented a systematic second-order relativistic RMBPT study of excitation energies in Zn-like ions with nuclear charges $Z=30-100$. Two alternative treatments of the Breit interaction are investigated. In the first version, we omit Breit contributions to the Dirac-Fock potential and evaluate Coulomb and Breit-Coulomb corrections through second order perturbatively. In the second version, we include both Coulomb and Breit contributions to the Dirac-Fock potential and then treat the residual Breit and Coulomb interactions perturbatively. Results obtained from the two versions are compared and discussed. Good agreement of

our RMBPT data with other accurate experimental measurements leads us to conclude that the RMBPT method provides accurate data for Zn-like ions. Results from the present calculations provide benchmark values for future theoretical and experimental studies of the zinc isoelectronic sequence.

ACKNOWLEDGMENTS

The work of W.R.J. and U.I.S. was supported in part by National Science Foundation Grant No. PHY-04-56828. The work of M.S.S. was supported in part by National Science Foundation Grant No. PHY-04-57078.

[1] Y. Liu, R. Hutton, Y. Zou, M. Andersson, and T. Brage, J. Phys. B **39**, 3147 (2006).
[2] M. S. Safronova, W. R. Johnson, and U. I. Safronova, Phys. Rev. A **53**, 4036 (1996).
[3] U. I. Safronova, W. R. Johnson, and H. G. Berry, Phys. Rev. A **61**, 052503 (2000).
[4] U. I. Safronova, W. R. Johnson, D. Kato, and S. Ohtani, Phys. Rev. A **63**, 032518 (2001).
[5] U. I. Safronova, W. R. Johnson, M. Safronova, and J. R. Albritton, Phys. Rev. A **66**, 022507 (2002).
[6] J. Reader and G. Luther, Phys. Rev. Lett. **45**, 609 (1980).
[7] N. Acquista and J. Reader, J. Opt. Soc. Am. B **1**, 649 (1984).
[8] J. F. Seely, J. O. Ekberg, C. M. Brown, U. Feldman, W. E. Behring, J. Reader, and M. C. Richardson, Phys. Rev. Lett. **57**, 2924 (1986).
[9] E. Hinnov, P. Beiersdorfer, R. Bell, J. Stevens, S. Suckewer, S. von Goeler, A. Wouters, D. Dietrich, M. Gerassimenko, and E. Silver, Phys. Rev. A **35**, 4876 (1987).
[10] U. Litzen and J. Reader, Phys. Rev. A **36**, 5159 (1987).
[11] S. S. Churilov, A. N. Ryabtsev, and J.-F. Wyart, Phys. Scr. **38**, 326 (1988).
[12] S. S. Churilov, Opt. Spectrosc. **93**, 826 (2002).
[13] J. Sugar, V. Kaufman, D. H. Balk, and Y.-Ki Kim, J. Opt. Soc. Am. B **8**, 1795 (1991).
[14] P. Indelicato and J. P. Desclaux, Phys. Rev. A **42**, 5139 (1990).
[15] J. Sugar, V. Kaufman, and W. L. Rowan, J. Opt. Soc. Am. B **10**, 799 (1993).
[16] S. B. Utter, P. Beiersdorfer, and E. Träbert, Can. J. Phys. **81**, 911 (2004).
[17] E. Träbert, P. Beiersdorfer, and H. Chen, Phys. Rev. A **70**, 032506 (2004).
[18] E. Biémont, P. Quinet, and B. C. Fawcett, Phys. Scr. **39**, 562 (1989).
[19] K. T. Cheng and R. A. Wagner, Phys. Rev. A **36**, 5435 (1987).
[20] E. Biémont, At. Data Nucl. Data Tables **43**, 163 (1989).
[21] C. Brown, J. Seely, D. Kania, B. Hammel, C. Back, R. Lee, A. Bar-Shalom, and W. Behring At. Data Nucl. Data Tables **58**, 203 (1994).
[22] H. S. Chou, H. C. Chi, and K. N. Huang, Phys. Rev. A **49**, 2394 (1994).
[23] M. J. Vilkas and Y. Ishikawa, Phys. Rev. A **72**, 032512 (2005).
[24] S. A. Blundell, Phys. Rev. A **47**, 1790 (1993).
[25] M. H. Chen, K. T. Cheng, W. R. Johnson, and J. Sapirstein, Phys. Rev. A **74**, 042510 (2006).
[26] W. R. Johnson, S. A. Blundell, and J. Sapirstein, Phys. Rev. A **37**, 307 (1988).
[27] P. J. Mohr, Ann. Phys. (N.Y.) **88**, 26 (1974).
[28] P. J. Mohr, Ann. Phys. (N.Y.) **88**, 52 (1974).
[29] P. J. Mohr, Phys. Rev. Lett. **34**, 1050 (1975).
[30] U. I. Safronova and A. F. Shestakov, *Relativistic and Radiative effects in Atoms and Ions* (USSR Academy of Science, Moscow, 1983), pp. 58–88.
[31] L. D. Landau and E. M. Lifshitz, *Quantum Mechanics-Non-Relativistic Theory* (Pergamon Press, London, 1963), p. 281.
[32] W. R. Johnson, S. A. Blundell, and J. Sapirstein, Phys. Rev. A **37**, 2764 (1988).
[33] A. Derevianko, Phys. Rev. A **65**, 012106 (2001).
[34] A. Kreuter, C. Becher, G. P. T. Lancaster, A. B. Mundt, C. Russo, H. Häffner, C. Roos, W. Hänsel, F. Schmidt-Kaler, R. Blatt *et al.*, Phys. Rev. A **71**, 032504 (2005).
[35] V. A. Dzuba, V. V. Flambaum, and M. S. Safronova, Phys. Rev. A **73**, 022112 (2006).